

12-2018

Radiative Heat Transfer Analysis of Railroad Bearings for Wayside Thermal Detector Optimization

James Alexandro Aranda
The University of Texas Rio Grande Valley

Follow this and additional works at: <https://scholarworks.utrgv.edu/etd>



Part of the [Mechanical Engineering Commons](#)

Recommended Citation

Aranda, James Alexandro, "Radiative Heat Transfer Analysis of Railroad Bearings for Wayside Thermal Detector Optimization" (2018). *Theses and Dissertations*. 417.
<https://scholarworks.utrgv.edu/etd/417>

This Thesis is brought to you for free and open access by ScholarWorks @ UTRGV. It has been accepted for inclusion in Theses and Dissertations by an authorized administrator of ScholarWorks @ UTRGV. For more information, please contact justin.white@utrgv.edu, william.flores01@utrgv.edu.

RADIATIVE HEAT TRANSFER ANALYSIS OF RAILROAD BEARINGS
FOR WAYSIDE THERMAL DETECTOR OPTIMIZATION

A Thesis

by

JAMES ALEXANDRO ARANDA

Submitted to the Graduate College of
The University of Texas Rio Grande Valley
In partial fulfillment of the requirements for the degree of
MASTER OF SCIENCE IN ENGINEERING

December 2018

Major Subject: Mechanical Engineering

RADIATIVE HEAT TRANSFER ANALYSIS OF RAILROAD BEARINGS
FOR WAYSIDE THERMAL DETECTOR OPTIMIZATION

A Thesis
by
JAMES ALEXANDRO ARANDA

COMMITTEE MEMBERS

Dr. Constantine Tarawneh
Chair of Committee

Dr. Stephen Crown
Committee Member

Dr. Robert Jones
Committee Member

Jazmin Ley
Committee Member

December 2018

Copyright © 2018 James Alexandro Aranda

All Rights Reserved

ABSTRACT

Aranda, James Alexandro, Radiative Heat Transfer Analysis of Railroad Bearings for Wayside Thermal Detector Optimization. Master of Science in Engineering (MSE), December, 2018, 85 pp., 14 tables, 48 figures, 22 references

Wayside hot-box detectors (HBDs) are devices that are currently used to evaluate the health of railcar components including bearings, axles, and brakes by monitoring their temperatures. While HBDs have been instrumental in reducing some train derailments in the past few decades, the number of non-verified bearing removals has increased significantly. In general, HBDs tend to underestimate bearing temperatures in both field service and in laboratory testing, which is not surprising considering the simple two-point calibration method that is used to calibrate these devices. Because of this, different calibrations were compared and analyzed including two-point, three-point, and multi-point calibrations. Analysis of the results also suggests that the scanning location significantly affects the temperature measurement. The work in this thesis summarizes how an optimized calibration technique along with proper IR sensor alignment can markedly improve the accuracy and precision of HBD temperature measurements.

DEDICATION

This work is dedicated to my loving family and to all the friends I have had the honor of meeting throughout the years. My father, James, for inspiring a love for engineering in me. My mother, Beatrice, for always offering love and support. My sister, Christa, for always believing in me. To my friends, for always offering encouragement. None of this would have been possible without all of you. I cannot thank you enough.

ACKNOWLEDGEMENTS

I would like to thank my research advisor, Dr. Constantine Tarawneh, for giving me the opportunity to be a part of this wonderful research team. You have invested so much time and effort into seeing your students succeed and reach their career goals in life. You have always pushed me to become a better engineer and inspired me to always do my best. I have learned so much from you and how to become a leader that leads by example. I hope one day I can follow in your footsteps and obtain my doctoral degree because I know that this is what you have always wanted for me to do.

I would also like to thank Dr. Jones and Dr. Crown for your support throughout the years. Not only have I learned so much about engineering from you, but I have also learned how to be a better person. I would like to extend this thanks to Ms. Jazmin Ley, whose advice has helped me throughout the years.

And to the friends I have made at the UTCRS, thank you. Your friendship and encouragement have been invaluable. I would like to express my deepest gratitude.

Finally, this study was made possible by funding provided by The University Transportation Center for Railway Safety (UTCRS), through a USDOT Grant No. #DTRT 13-G-UTC59

DISCLAIMER

The contents of this thesis reflect the views of the authors, who are responsible for the facts and the accuracy of the information presented herein. This document is disseminated under the sponsorship of the U.S. Department of Transportation's University Transportation Centers Program, in the interest of information exchange. The U.S. Government assumes no liability for the contents or use thereof.

TABLE OF CONTENTS

	Page
ABSTRACT.....	iii
DEDICATION.....	iv
ACKNOWLEDGEMENTS.....	v
DISCLAIMER.....	vi
TABLE OF CONTENTS.....	vii
LIST OF TABLES.....	x
LIST OF FIGURES.....	xi
CHAPTER I. BACKGROUND & INTRODUCTION.....	1
1.1 Introduction.....	1
1.2 Bearing Nomenclature and Common Field Test Practices.....	2
1.3 Current Problems and Developments in Wayside Hot Box Detector Technologies.....	5
CHAPTER II. WAYSIDE HOT BOX DETECTOR SIMULATOR DESIGN AND FABRICATION.....	12
2.1 Wayside Hot Box Detector Simulation Concept.....	12
2.2 Pneumatic System Overview.....	15
2.3 Electrical System Overview.....	16
2.4 Programming.....	18
CHAPTER III. EXPERIMENTAL SETUP AND PROCEDURES.....	20

3.1	Field Test Setup.....	20
3.2	Laboratory Test Setup	21
3.2.1	Single Bearing Test Rig	21
3.2.2	Laboratory Infrared Temperature Sensor.....	23
3.2.3	Infrared Scanning Profile	24
3.2.4	Test Parameters.....	25
3.2.5	Test Bearing Conditions	26
3.2.6	Data Acquisition	28
3.2.7	Static Testing of Infrared Sensor	28
3.2.8	Bearing Emissivity Values.....	30
CHAPTER IV. RADIATIVE THERMAL ANALYSIS OF RAILROAD BEARINGS		32
4.1	Bearing Temperature Behavior	32
4.2	Bearing Temperature Profile	33
4.3	Laboratory Data Analysis.....	36
4.3.1	Raw Laboratory Data	36
4.3.2	Sensor Error Plots	39
4.3.3	HBD Simulator Sensor Error Tables for Laboratory Testing	42
4.4	Field Test Data Analysis	43
4.4.1	Raw Field Test Data.....	43
4.4.2	HBD Sensor Error Tables for Field Testing	44
CHAPTER V. HOT BOX DETECTOR (HBD) OPTIMIZATION		46
5.1	Laboratory Data Optimization	46

5.1.1	Calibration Methods.....	46
5.1.2	Coefficient of Determination and Root-Mean-Squared Error	49
5.1.3	Calibrated Laboratory HBD Simulator Data	52
5.1.4	Other Calibration Methods	56
5.2	Field Data Optimization.....	60
5.2.1	Calibration Methods.....	60
5.2.2	Coefficient of Determination and Root-Mean-Squared Error	61
5.2.3	Calibrated Field Service HBD Data.....	64
CHAPTER VI. CONCLUSIONS AND RECCOMENDATIONS.....		66
APPENDIX A.....		68
APPENDIX B		80
REFERENCES		83
BIOGRAPHICAL SKETCH		85

LIST OF TABLES

	Page
Table 1. Bearing dimensions and class [8]	3
Table 2. Speeds used for test bearings in this study	26
Table 3. Descriptions of the bearing laboratory testing performed for this study	27
Table 4. Infrared (IR) sensor oven test results [19]	29
Table 5. Emissivity study results [19].....	31
Table 6. Laboratory bearing temperature error for unloaded (empty railcar) bearings	42
Table 7. Laboratory bearing temperature error for loaded (full railcar) bearings	43
Table 8. Raw field-test bearing temperature error	45
Table 9. Coefficient of determination (R^2) and root-mean-squared-error (RMSE) for various calibrations	50
Table 10. Laboratory bearing temperature error for unloaded (empty railcar) bearings	55
Table 11. Laboratory bearing temperature error for loaded (full railcar) bearings	55
Table 12. Coefficient of determination (R^2) and root-mean-squared-error (RMSE) for other calibrations explored in this study	59
Table 13. Coefficient of determination (R^2) and root-mean-squared-error (RMSE) for various calibrations utilized.....	62
Table 14. Calibrated field-test bearing temperature error.....	65

LIST OF FIGURES

	Page
Figure 1. Depiction of a wayside Hot-Box Detector (HBD) [6].....	2
Figure 2. Double tapered-roller bearing exploded view [7]	3
Figure 3. Class F (pictured left) and Class K (pictured right) bearings	5
Figure 4. Photograph of a wayside Hot-Box Detector system [10]	6
Figure 5. Typical infrared sensor scanning location for field wayside hot-box detectors (HBDs) [16].....	8
Figure 6. Hot-Box Detector simulation system. From A through H there is the cylinder [A], the quick exhaust valve [B], the cart [C] with the sensor [D] attached, the control box [E], the filter [F] for the pneumatic system followed by the regulator [G] and the lubricator [H].13	13
Figure 7. Top-view of the cart that transports the IR sensor showing the markings on the cart that correspond to the four regions of interest.	13
Figure 8. Infrared scanning locations from left to right: inboard seal, inboard raceway, spacer ring, and outboard raceway.....	14
Figure 9. Infrared scanning locations on the bearing.....	14
Figure 10. Electrical system schematic diagram.....	16
Figure 11. Electrical system schematic.....	17
Figure 12. HBD simulator programming flowchart	19
Figure 13. Field-test instrumentation setup where each red dot represents an onboard bayonet-style-K type thermocouple.....	21
Figure 14. Single Bearing Tester (SBT) with annotations.....	22
Figure 15. Bearing thermocouple locations, where each red dot represents a standard K-type thermocouple and the black dots represent spring-loaded bayonet-style K-type thermocouples	23
Figure 16. MICRO-EPSILON infrared (IR) temperature sensor.....	24

Figure 17. Typical IR sensor scanning profile.....	25
Figure 18. Outer ring (cup) spall from Exp. 198C (pictured left) and inner ring (cone) spall from Exp. 202A (pictured right).....	27
Figure 19. Oven test experimental setup [19].....	29
Figure 20. Overhead schematic of the setup used for bearing emissivity study. [19]	31
Figure 21. Examples of bearing cups used for emissivity testing includes brushed surface (left), moderately used surface (center), and heat-tinted rusted surface (right).....	31
Figure 22. Class F and K bearing average operating temperatures for fully-loaded (100% load) and unloaded (17% load corresponding to empty railcar) conditions at various speeds ..	33
Figure 23. Bearing temperature profiles for an unloaded and loaded control bearing at 64 km/h (40 mph) and 89 km/h (55 mph).....	34
Figure 24. FLIR camera thermal image of tapered-roller bearing (side view).....	35
Figure 25. Laboratory raw HBD simulator temperature versus onboard bayonet thermocouple temperature for the bearing outboard (OB) raceway location	37
Figure 26. Laboratory raw HBD simulator temperature versus onboard bayonet thermocouple temperature for the bearing spacer ring location	37
Figure 27. Laboratory raw HBD simulator temperature versus onboard bayonet thermocouple temperature for the bearing inboard (IB) raceway location.....	38
Figure 28. Laboratory raw HBD simulator temperature versus onboard bayonet thermocouple temperature for the bearing inboard (IB) seal location.....	38
Figure 29. Infrared (IR) sensor error compared to the top two thermocouple average temperature for the outboard raceway region	39
Figure 30. Infrared (IR) sensor error compared to the top two thermocouple average temperature for the spacer ring region	40
Figure 31. Infrared (IR) sensor error compared to the top two thermocouple average temperature for the inboard raceway region	40
Figure 32. Infrared (IR) sensor error compared to the top two thermocouple average temperature for the inboard seal region	41
Figure 33. Raw field-test wayside HBD temperature versus onboard thermocouple temperature	44
Figure 34. Two-point and three-point calibrations using data acquired by the laboratory HBD simulator	48

Figure 35. Calibration using the trendline through all data collected by the laboratory HBD simulator	48
Figure 36. All laboratory data root-mean-squared-error (RMSE) comparison for various calibrations at each scanning location.....	51
Figure 37. All laboratory data coefficient of determination (R^2) for various calibrations at each scanning location	52
Figure 38. Calibrated laboratory HBD simulator temperature versus onboard bayonet thermocouple temperature for the bearing outboard (OB) raceway location	53
Figure 39. Calibrated laboratory HBD simulator temperature versus onboard bayonet thermocouple temperature for the bearing spacer ring location	53
Figure 40. Calibrated laboratory HBD simulator temperature versus onboard bayonet thermocouple temperature for the bearing inboard (IB) raceway location.....	54
Figure 41. Calibrated laboratory HBD simulator temperature versus onboard bayonet thermocouple temperature for the bearing inboard (IB) seal location	54
Figure 42. Various two-point calibrations for laboratory-acquired data	57
Figure 43. Root-mean-squared-error (RMSE) for other two-point calibration methods that were explored for this study	59
Figure 44. Two-point and three-point calibrations using field-test data.....	60
Figure 45. Calibration equation using the trendline through all data collected during the in-service field test	61
Figure 46. Root-mean-squared-error (RMSE) comparison for all test cases in the field test.....	63
Figure 47. Coefficient of determination (R^2) comparison for all test cases in the field test.....	63
Figure 48. Calibrated field-test wayside HBD temperature versus onboard thermocouple temperature	64

CHAPTER I

BACKGROUND & INTRODUCTION

1.1 Introduction

Bearing health monitoring systems are devices used by the railroad industry to identify problematic bearings so they can be safely removed from service; thus, preventing catastrophic bearing failures that can lead to costly train derailments. The railroad industry currently utilizes two wayside detection systems to monitor the health of freight railcar bearings in service: The Trackside Acoustic Detection System (TADS™) and the wayside Hot-Box Detector (HBD). TADS™ uses wayside microphones to detect and alert the conductor of high-risk defects [1]. Many defective bearings may never be detected by TADS™ due to the fact that a high-risk defect is considered a spall which spans more than 90% of a bearing's raceway, and there are less than 20 systems in operation throughout the United States and Canada [2]. Wayside Hot-Box Detectors (HBDs) are devices that sit on the side of the rail tracks and use non-contact infrared sensors to determine the temperature of the train bearings as they roll over these detectors. HBDs are the most common bearing health monitoring system utilized in the U.S. with over 6,000 of these devices spread across the nation's railways [3]. Typically, HBDs are positioned around 24 to 48 km (15 to 30 mi) apart along the rail track [4]. As each freight car passes, the HBDs scan the bottom surface of the railroad bearings, recording infrared temperature measurements of the bearings as well as the ambient temperature from the surroundings. An alarm will be triggered if the difference between the infrared temperature of

the bearing surface and the ambient temperature of the surroundings exceeds a predetermined threshold. One set of common criteria that will trigger an alarm is as follows: (1) if a bearing is operating at a temperature greater than 94.4°C (170°F) above the ambient temperature or (2) if a bearing is operating at a temperature greater than 52.8°C (95°F) above the temperature of the bearing that shares the same axle [5].

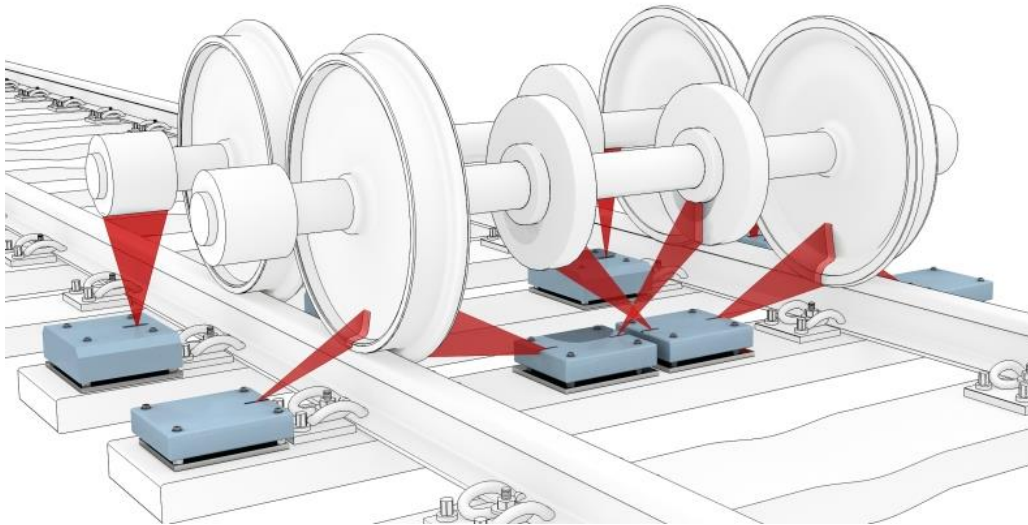


Figure 1. Depiction of a wayside Hot-Box Detector (HBD) [6]

1.2 Bearing Nomenclature and Common Field Test Practices

The standard bearing used in the modern freight railway industry is the double tapered-roller bearing. An exploded view that contains each element of this type of bearing is shown in Figure 2. These bearings are press fit on either end of a solid axle and secured via an end cap. The side of the bearing approaching this end cap is often referred to as the outboard side of the bearing while the side closer to the railcar is commonly referred to as the inboard side of the bearing. Each bearing contains two inner rings, also called cones, with rollers that are separated by a cage. This cage, manufactured from either steel or a polymer, ensures that the rollers are kept apart at a fixed distance. A spacer ring is also installed between the two inner ring assemblies. All of the aforementioned components are housed within the bearing outer ring, also

called the bearing cup. The areas where the bearing cup meets the rollers are referred to as the cup raceways. Each bearing is closed with seals to prevent any contaminants from reaching the lubrication inside the bearing.

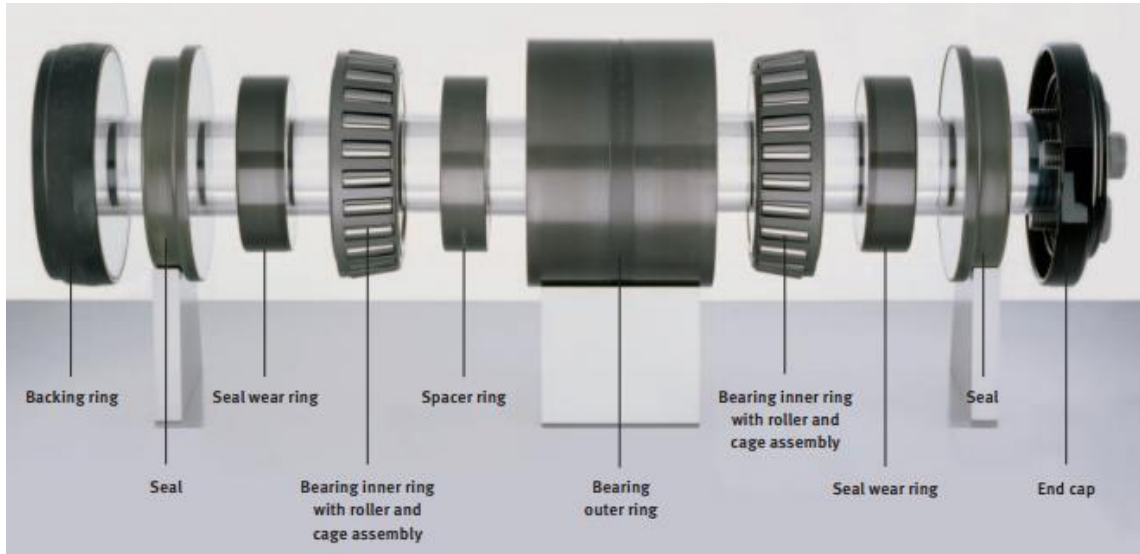


Figure 2. Double tapered-roller bearing exploded view [7]

Table 1. Bearing dimensions and class [8]

Bearing Class	Nominal Journal Diameter × Width [inch]*	Nominal Bearing Load [kN/kips]	Nominal Horizontal Distance from Rail Gage Point to Inboard Edge of Cup [inch]*	Nominal Horizontal Distance from Rail Gage Point to Center of Cup [inch]*
E	6 × 11	117.0/26.3	7.5	10.75
F	6 ½ × 12	153.0/34.4	7.6	11.25
G	7 × 12	169.0/38.0	7.6	11.25
K	6 ½ × 9	153.0/34.4	8.1	11.25

***Dimensions are normally specified in inches**

The Association of American Railroads (AAR) classifies bearings according to their size and load carrying capacity. Four of the most common AAR bearing classes are shown in Table 1.

Two of these bearing classes, Class K and Class F, share the same bore size and loading capacity but differ in length. In comparison to these two bearing classes, Class E bearings have a smaller bore size and capacity while Class G bearings have a greater bore size and loading capacity.

HBDs use infrared sensors to measure the temperature of the bottom of the bearing cup surface. These sensors are usually fixed to scan a bearing a certain distance adjacent to the track. Most wayside HBDs that are currently deployed in the field are configured to scan the inboard edge of the bearing cup at 18.42 cm (7.25 in) from the rail gage [8]. However, due to changes in bearing dimensions, an HBD that is configured to scan the inboard edge of the bearing may scan a different region of the bearing depending on the bearing class. A summary of the distance from the rail gage to common locations on the bearing is provided in Table 1. This table shows that for Class F, Class G, and Class K bearings, although the distance from the rail gage to the center of the bearing cup is identical, the distance to the inboard edge of the cup is markedly different. Between Class K and Class F bearings, the distance from the rail gage to the edge of the cup differs by 1.27 cm ($\frac{1}{2}$ in). This latter fact is important in the study presented in this thesis because the study focuses mainly on the operating temperatures of Class K and Class F bearings as measured by wayside detection systems. The physical differences between these bearing classes can be seen in Figure 3.



Figure 3. Class F (pictured left) and Class K (pictured right) bearings

1.3 Current Problems and Developments in Wayside Hot Box Detector Technologies

Due to the catastrophic consequences of unreliable condition monitoring systems, it is critical to examine the effectiveness of wayside HBDs. Variables such as bearing class and IR scanning location may affect the accuracy of HBD temperature data. Changes in these variables may cause the HBD system to greatly underpredict or overpredict the temperatures of these railroad bearings. In the event of an overpredicted temperature measurement, a healthy bearing may be falsely flagged as defective and will be removed from service. Upon inspection, if no defects or other problems are found, the bearing is classified as “non-verified”. These non-verified bearings lead to delays and unnecessary train stoppages, which cost both time and money. In a study performed from 2001 to 2007, Amsted Rail found that nearly 40% of bearings that were removed from service were classified as “non-verified”. In the event that an HBD greatly underpredicts the temperature of a bearing that is overheating, and an alarm is not triggered, catastrophic failure may occur. It was found that from 2010 to 2016, wayside HBDs

have failed to detect 119 severely defective bearings throughout the United States and Canada, all of which led to catastrophic derailments [9].

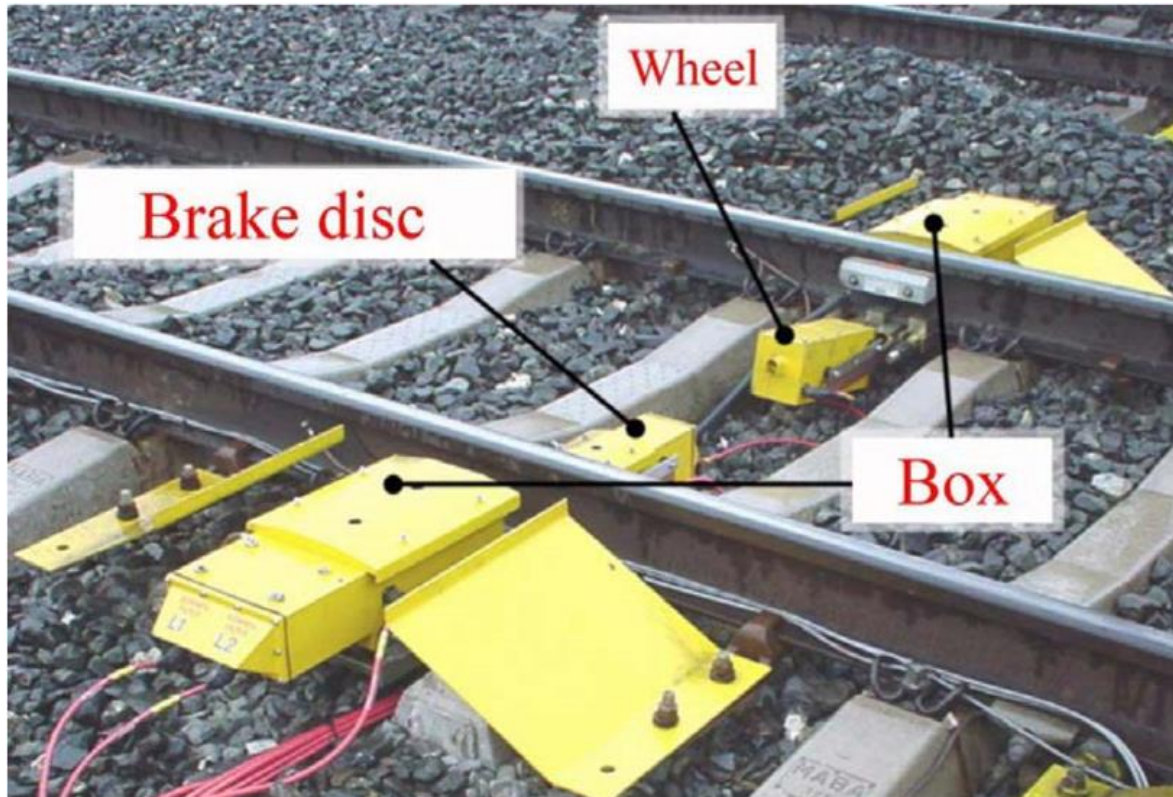


Figure 4. Photograph of a wayside Hot-Box Detector system [10]

Bearing condition monitoring technologies can be divided into two categories: predictive and reactive systems. Predictive systems are capable of analyzing the condition of the equipment in order to predict any forthcoming failures. Alternatively, reactive systems detect faults on vehicles as they occur in order to prevent any further damage [11]. One major characteristic of wayside HBDs is that they are often used as a reactive bearing condition monitoring system. A hot-box detector is intended to be able to detect the heat radiating from a bearing shortly before failure from overheating. The rate of heating in this time can cause components in the bearing to rise to temperatures of up to 800°C (1472°F) in a span of nearly 25 minutes [12]. The addition of more detectors on the track has been implemented in the past, however, this has had a limited

effect due to the rapid failure modes associated with overheated bearings [11]. In fact, bearing failure has occurred within 96 seconds of passing a hot-box detector without triggering an alarm [13]. Due to events such as these, effort has been made to improve wayside HBD technology by using it as a predictive condition monitoring system. In 1997, Canadian National began to track bearing temperatures to search for any signs of temperature increase between HBDs. By tracking individual bearing temperatures, hot bearings in danger of overheating can be predicted based on prior warm bearing readings [14]. In 2003, the Union Pacific Railroad in the U.S. planned to connect 1200+ wayside HBDs to create an integrated monitoring system [11]. Despite attempts to improve these devices, growing concerns still exist with regards to the overall efficacy of wayside HBDs.

As previously mentioned, the most common way of assessing bearing health with wayside HBDs is to see if the bearing temperature exceeds a predetermined threshold. However, factors such as train speed, braking events, and calibration errors may affect the accuracy of HBD temperature measurements. Because of this, Union Pacific started using a relative temperature performance system in 2002 to monitor bearing temperature performance. This process involves using statistics to divide wayside temperature data from the bearings in railcars into quartiles. These statistical groups are used to calculate a “K-Value”, which is used to quantify the deviation of a single bearing temperature from the rest of the bearings installed on a train. Using this method, it is possible to separate healthy bearings from defective bearings in a railcar with relatively low sensitivity to calibration and environmental factors [5].

Due to the errors present in modern HBD systems, the efficacy of HBDs were studied by the Transportation Technology Center, Inc. (TTCI) in 2013 at the Railroad Test Track (RTT) at Pueblo, Colorado. This study evaluated HBDs from four different vendors using four different

classes of bearings (Class K, F, E, and G). Other conditions that were varied were the scanning location of the infrared temperature measurement along the bearing and the scanning angle. The test bearings were equipped with onboard thermocouples for a continuous temperature reference. The results from the study indicated that HBD configurations that measure temperatures closer to the inboard raceway at a near vertical scan angle generally have improved results compared to bearings tested with other HBD configurations [15].

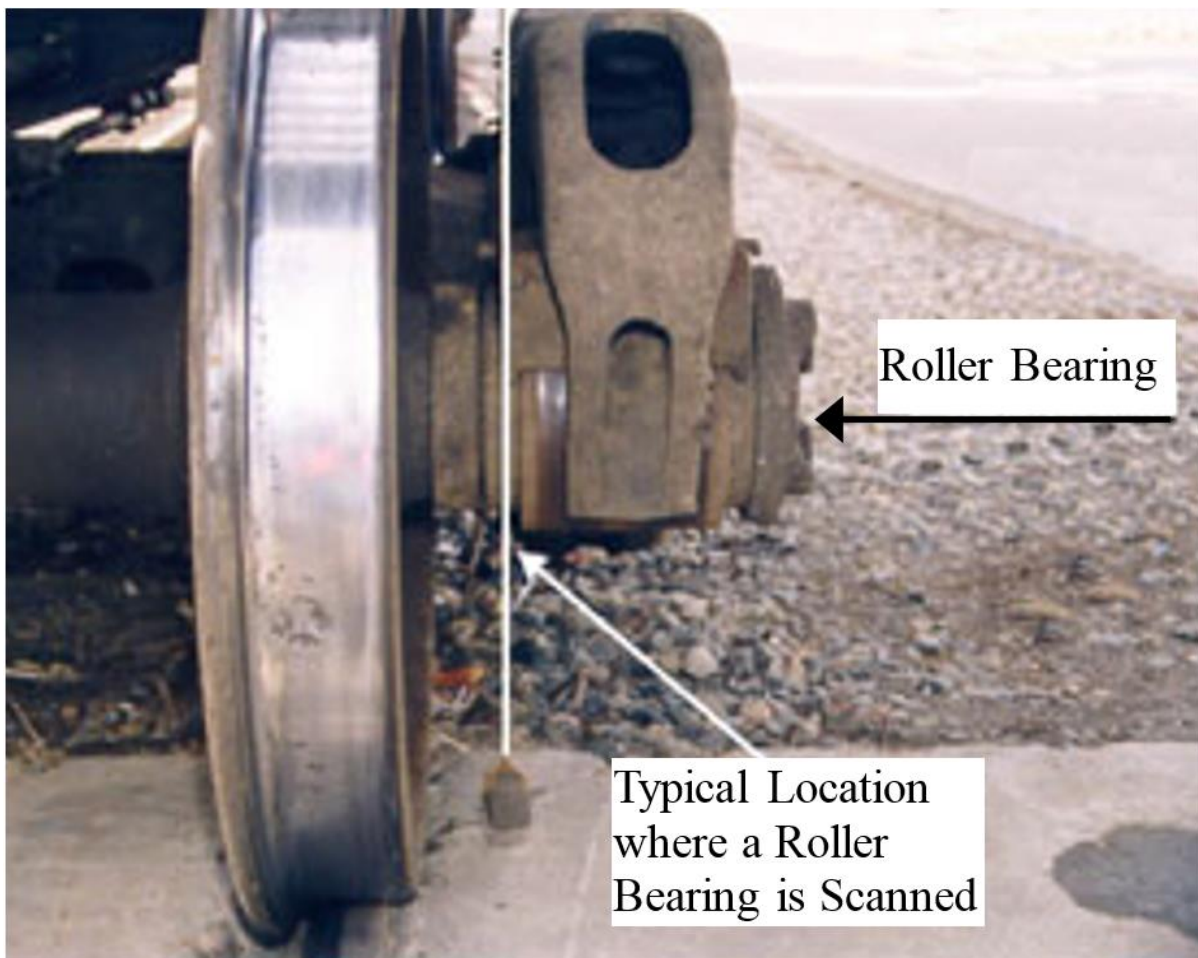


Figure 5. Typical infrared sensor scanning location for field wayside hot-box detectors (HBDs)

[16]

In the early 1990s, a Hot Bearing Specification Development Test was conducted by the Association of American Railroads (AAR) at TTCI in Pueblo, Colorado. The purpose of this test

was to use an adjustable aperture device on heated roller bearings to vary the amount of scanning time and scanning area for wayside HBDs in order to create recommended certification procedures for new truck and HBD designs. During the test, 71.12 cm (28") and 91.44 cm (36") wheels were outfitted with resistance heaters, temperature control equipment, and temperature measurement transducers. The aperture that was outfitted on the wayside HBDs during testing was adjustable in both the vertical and horizontal direction so that the scanning area can be modified. Various scanning areas were tested in order to generate computer-aided drawings that define the minimum unobstructed area in truck designs that is required for compatibility with current HBDs. To assist with the process of checking for obstructions that are caused by a truck design in a field setting, a laser system that simulates the HBD scan path was utilized. If this test did not provide proof that the truck met the required specifications, an additional compatibility test was conducted to determine the actual performance of the wayside HBDs in relation to any new truck design. Additionally, recommended certification processes for wayside HBDs were developed by creating computer generated drawings that define the area in which an HBD must be able to operate reliably [17].

Joint research between TTCI and the University of Illinois at Urbana-Champaign has been conducted using mathematical models and simulation to determine the optimum spacing between wayside HBDs in service. Data obtained from HBD systems that are currently in place were used to simulate potential HBD spacing scenarios. Additionally, the tradeoff between sensor deployment cost and sensor efficacy was studied. Using a subset of 27 cases of journal-burn off incidents that was reported by the Federal Railroad Administration from 2012 to 2016, the median distance to derailment was determined to be around 14.8 km (9.2 mi). It was determined that reducing the spacing between wayside HBDs to less than 14.8 km (9.2 mi) apart

could reduce the percentage of train derailments due to journal-burn off by 50%. However, after further analysis of different wayside HBD spacing distances, it was determined that there was little to no statistical advantage in a sensor spacing of 14.8 km (9.2 mi) as compared to 24.14 km (15 mi), making this the optimum distance between HBDs positioned on the track [18].

One development that is currently being studied is the use of alternative HBD scanning technologies. Using a multiple scan HBD system, eight temperature scans of different sections of the bearing can be used to generate a diagram of the temperature distribution across the bearing in both dimensions. If the bearing is seen to be overheating, the temperature profile can be analyzed to locate defective components. For example, if the outermost scans are 10 degrees hotter than the rest of the bearing, the problem inside the bearing may be located in the outboard raceway assembly. Another advantage of this system is redundancy, which is achieved by replacing one sensor with eight different sensors [8].

A number of studies that are a part of this thesis have been performed at the University Transportation Center for Railway Safety (UTCRS) at the University of Texas Rio Grande Valley (UTRGV) to assess the efficacy of wayside HBD systems. In order to perform this assessment, a dynamic single bearing test rig was developed that is capable of simulating train loads of up to 200 kN (45 kips) per bearing and speeds of up to 137 km/h (85 mph). Class F and K bearings are rated for a full-load of 153 kN (34.4 kips) per bearing and generally run at train speeds less than 113 km/h (70 mph). Additionally, an IR sensor with similar characteristics to those currently employed in most HBD systems was utilized. The sensor was launched underneath the bearing using a pneumatically powered cart-track system to take a dynamic temperature measurement similar to the measurements taken by HBDs in field service. Various conclusions have been drawn from these studies. One major finding showed that an IR

temperature measurement taken at the inboard (IB) raceway location of the bearing is both the most precise and accurate when compared to other IR scanning locations. Additionally, it was concluded that as the bearing operating temperature increased, the temperature error between onboard thermocouples and the IR temperature measurement increased for all scanning locations [19]. This finding was verified using field test data acquired prior to this study, which used 21 different HBDs deployed in the United States. In order to replicate a process frequently performed in industry, a two-point calibration was performed between the IR temperature sensor and onboard thermocouples [20]. This calibration significantly improved the results of all IR temperature data gathered. Although this two-point calibration yielded positive results, three-point calibrations and calibrations using even more points have not been examined in depth, which is a main focus of this study.

The study presented in this thesis will serve to assist in the evaluation of current bearing condition monitoring systems, which will further the advancement of safety technology in the railway industry. The effects of this study can help save the industry millions of dollars in property damage caused by train derailments and hundreds of man-hours lost from false bearing set-outs. The wayside HBD system that was developed is unprecedented and allows for the quick and efficient testing of a modern HBD setup in a laboratory setting. Data acquired from 21 HBDs deployed in the US have been used to validate this laboratory system. Furthermore, the principles behind the operation of the HBD system will be documented, which has never been detailed in previous work.

CHAPTER II

WAYSIDE HOT BOX DETECTOR SIMULATOR DESIGN AND FABRICATION

2.1 Wayside Hot Box Detector Simulation Concept

To simulate the wayside HBD in the laboratory setting, a specialized testing system was designed and built at the University of Texas Rio Grande Valley (UTRGV) by the University Transportation Center for Railway Safety (UTCRS). This system, shown in Figure 6, propels an IR sensor underneath the test bearing on the Single Bearing Tester at a prescribed speed. To accomplish this, a pneumatically actuated cart system was designed and fabricated which housed the IR sensor. This IR sensor was secured to an adjustable mount which allowed the sensor to be pushed underneath the bearing at different scanning locations. These scanning locations, pictured in Figure 7 through Figure 9, correspond to the outboard (OB) raceway, spacer ring, inboard (IB) raceway, and inboard seal regions of the bearing.

To control the cart assembly, the pneumatic cylinder is connected to a four-way valve that is controlled by an Arduino Uno R3. To calculate the traveling velocity of the cart, two pairs of IR break sensors were placed along the cart track. This setup was used to determine the time at which the cart passed two fixed locations, and this information was then used to calculate the cart velocity. Using the current setup, the sensor can travel at a maximum velocity of 11.3 km/h (7 mph). Although this speed is slower than real service conditions, the system is designed to provide a best-case scenario analysis. That is, if this lower speed results in significant error in the laboratory IR sensor, the error will be magnified in field service operation.

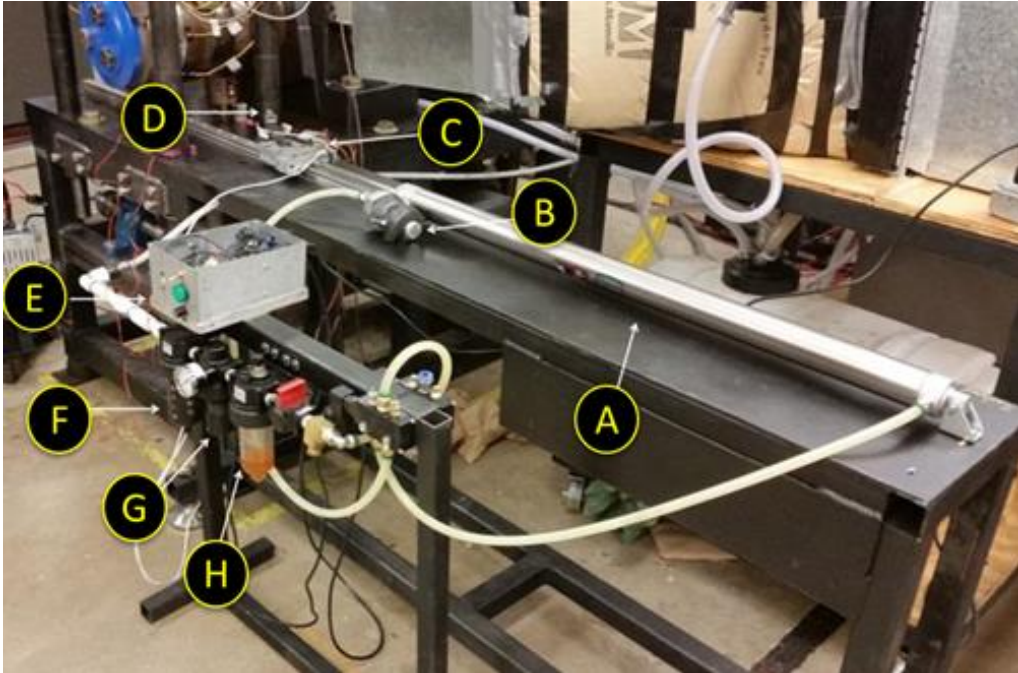


Figure 6. Hot-Box Detector simulation system. From A through H there is the cylinder [A], the quick exhaust valve [B], the cart [C] with the sensor [D] attached, the control box [E], the filter [F] for the pneumatic system followed by the regulator [G] and the lubricator [H].

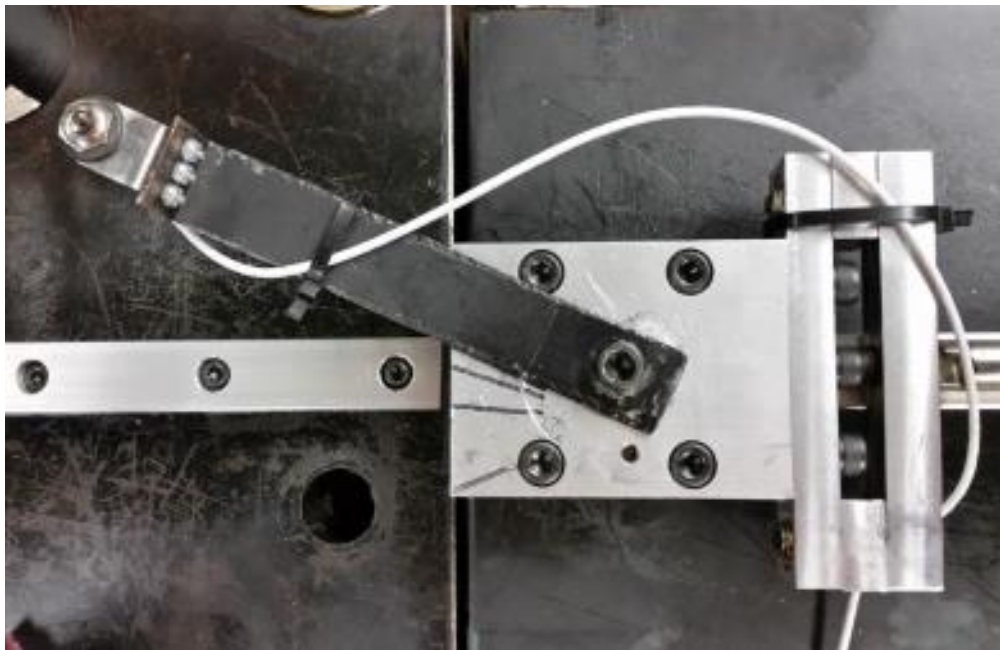


Figure 7. Top-view of the cart that transports the IR sensor showing the markings on the cart that correspond to the four regions of interest.

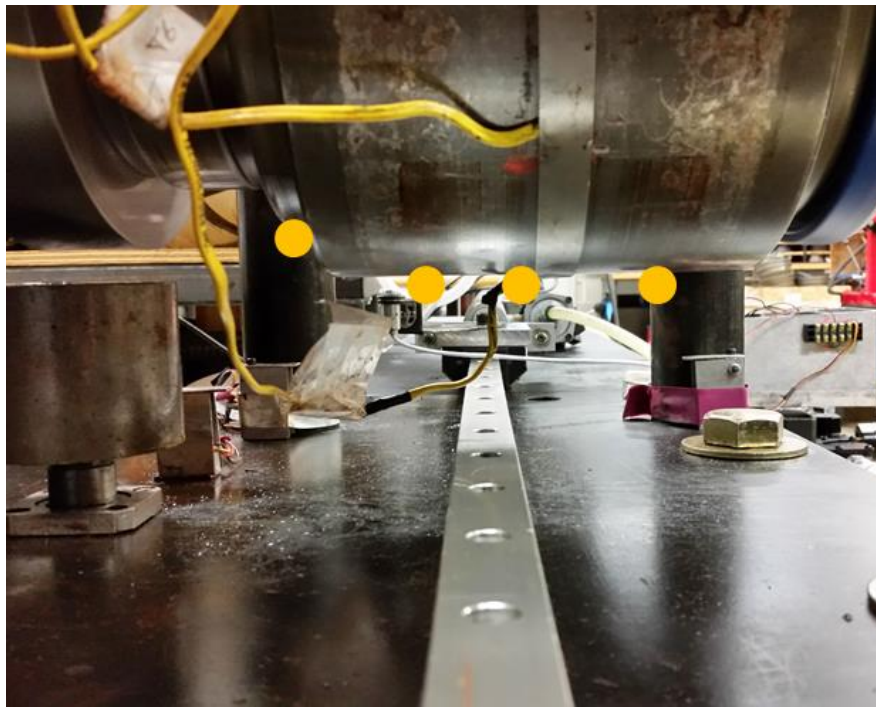


Figure 8. Infrared scanning locations from left to right: inboard seal, inboard raceway, spacer ring, and outboard raceway

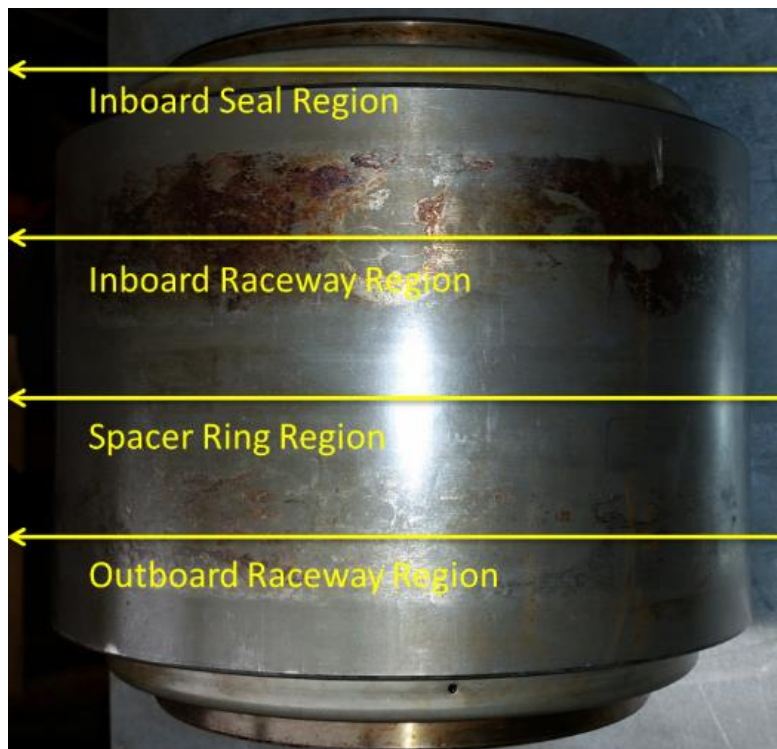


Figure 9. Infrared scanning locations on the bearing

2.2 Pneumatic System Overview

A picture of the wayside HBD simulation system is given in Figure 6, whereas, the components of this system are summarized in the schematic diagram of Figure 10. The entire pneumatic system has air supplied by a 227 L (60 gal) air tank with a 2.76 kW (3.7 hp) compressor. A filter (Parker 07F32BC) is used directly after the air tank to remove any contaminants from the air supply. Additionally, a regulator (Parker 07R313AC) is used to keep the air pressure in the system constant. A lubricator (Parker 07L 21BE8B) is placed before the four-way valve (Parker B512ADA53C) and the pneumatic cylinder to coat the internals of these components with an aerosolized stream of oil. The pneumatic cylinder (Clippard UDR-32-36-B) that is used is double acting, meaning air can be added to either side of the piston to extend or retract it. To extend the pneumatic cylinder, air is applied to the piston opposite to the IR sensor affixed to the cart, also called the cap-end. To quickly divert the air from the other end of the pneumatic cylinder, also called the rod-end, a quick exhaust valve (Parker 0R25N8) was installed with a silencer to suppress loud noises. The sudden impact of the cart system may damage the IR sensor when the piston slams into the rod end. To prevent this from occurring, after the cart has passed the two IR break sensors, air is applied to the rod-end side of the cylinder to slow the piston down. Additionally, a cushion is installed inside the rod-end of the pneumatic cylinder to dampen any impact forces and to decrease the sudden deceleration of the IR sensor cart.

Major Components

- 1 - double acting cylinder
- 2 - quick exhaust
- 3 - silencer
- 4 - 5/2 vlv, sol opr, spring return
- 5 - lubricator
- 6 - regulator
- 7 - filter

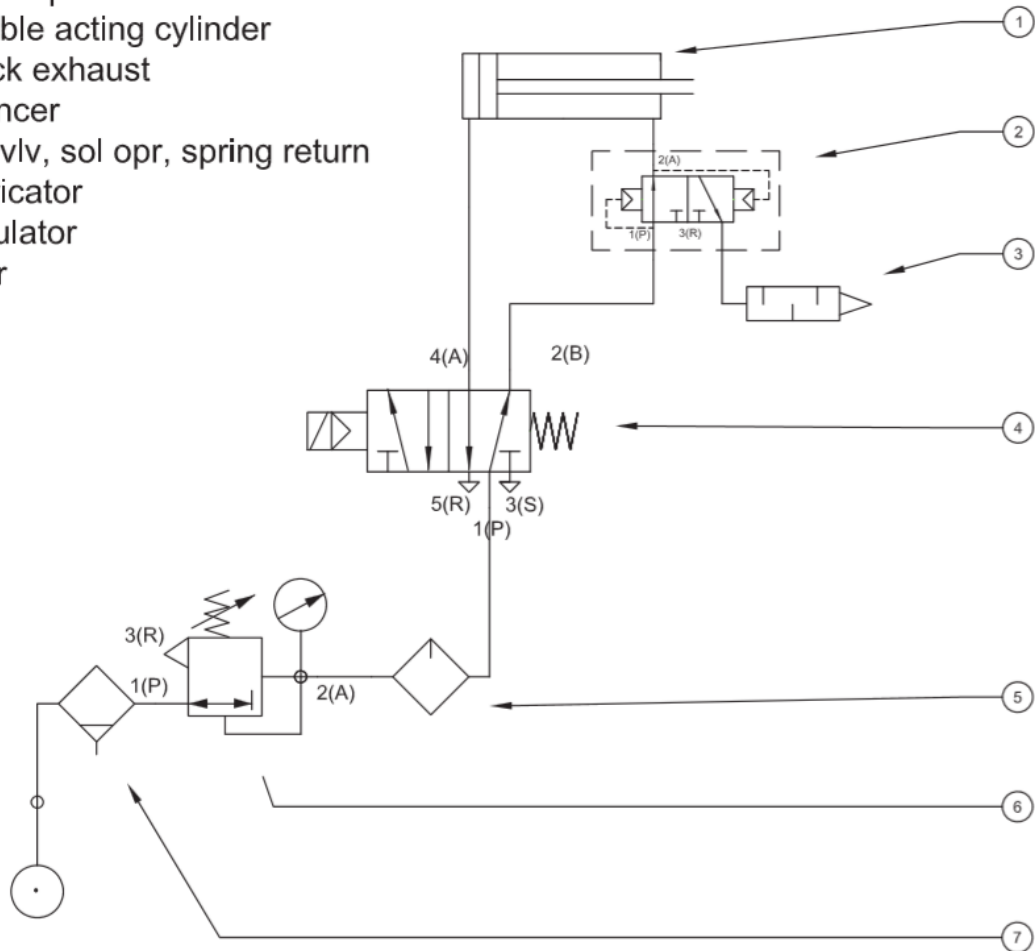


Figure 10. Electrical system schematic diagram

2.3 Electrical System Overview

To regulate the four-way valve of the pneumatic system, an Arduino Uno R3 microprocessor is utilized. Figure 11 is a schematic diagram of the electrical system. To switch the four-way valve, a single pole double-throw 120-volt relay is used. The control coil for this relay operates on 5 volts. To operate the coil for the relay, an NPN transistor is used as a switch to send a 5-V signal from the Arduino. The relay and four-way valve are operated by solenoids, which have large inductances. These inductances send a large, sudden voltage spike through the system after a voltage is applied or removed quickly. To prevent any damage to the Arduino or

surrounding components, a diode is placed in parallel. The 120-V section of the circuit includes all the components in series with the four-way solenoid valve and the relay. These parts include a fuse, which protects other components from overcurrent, and a switch, which turns the system on and off. A safety light was also installed to let the user know that the system is on and to keep hands away from the pneumatic system.

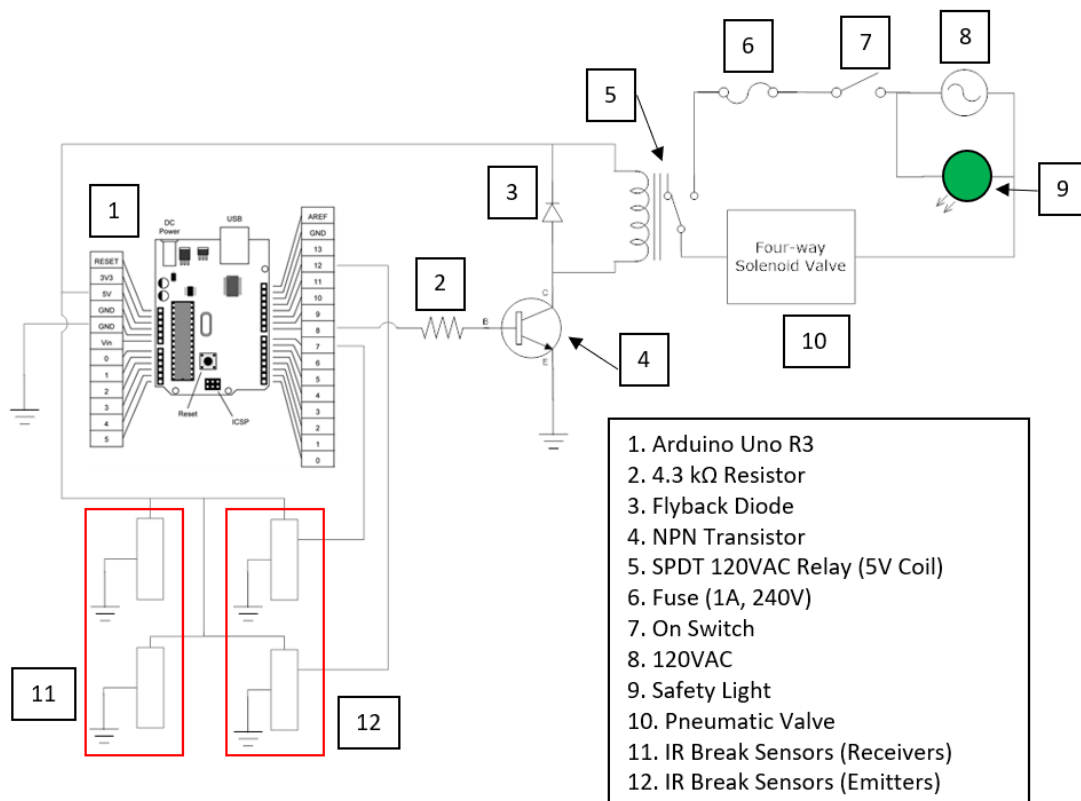


Figure 11. Electrical system schematic

The Arduino Uno R3 is also used to manage the inputs from the IR break sensors. To operate these, 5-V is sent to power the emitters and the sensors are aligned so that each emitter is sending a signal to its corresponding receiver. In turn, the receiver sends a signal to the Arduino indicating that the sensors are aligned with no obstructions in between. If the linear path between a pair of sensors is broken, the receiver stops sending its signal to the Arduino which indicates that something has passed in between the IR sensors—in this case the IR sensor cart.

2.4 Programming

A flowchart that describes the programming of the Arduino Uno R3 is presented in Figure 12. The first step of the programming activates the four-way valve to apply pressure to the cap-end side of the pneumatic cylinder which extends it. The program then waits for the first IR sensor to be broken. After the first IR sensor is broken, the time is displayed and stored for future use. As the pneumatic cylinder is still extending, the cart breaks the second set of IR sensors. The time is then stored again and the valve is switched to supply air to the rod-end of the pneumatic cylinder. The two time values recorded, as the IR sensor cart passes by the two sets of IR break sensors, are subtracted from each other and divided by the distance between the two sets of IR break sensors to obtain velocity of the cart. Finally, once the valve is switched to retract the pneumatic cylinder, the program is set to delay for 30 seconds. After this delay, the process is complete. For each test, this process was repeated three times and the average bearing temperature from the three trials was calculated. To break the programming loop after the test is complete, the power is cut-off by the machine operator through the mechanical power switch mentioned earlier.

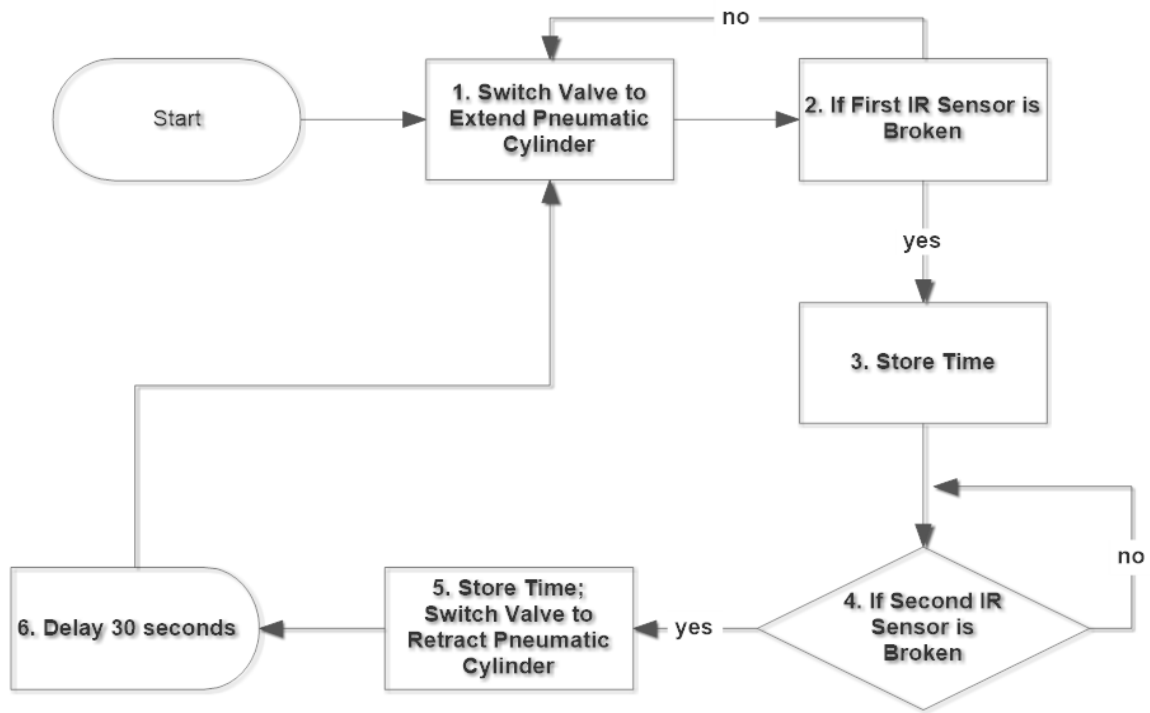


Figure 12. HBD simulator programming flowchart

CHAPTER III

EXPERIMENTAL SETUP AND PROCEDURES

3.1 Field Test Setup

A field test, performed in fall of 2008, was conducted to investigate the warm bearing trending phenomenon experienced in freight railcar service [21]. The acquired data was also used to characterize the efficacy of wayside hot-box detectors (HBDs). This test was conducted along more than 483 km (300 mi) stretch of track and passed over 21 different HBDs along the way. Two freight cars, one loaded and one unloaded, were tested with a total of 16 double-tapered roller bearings. Of the 16 bearings, 14 were Class F while the other two were Class K. Of the Class F bearings, three were previously removed from field service due to an outboard inner ring (cone) spall, an inboard outer ring (cup) defect, and a loose cone-cage assembly. Additionally, two of the Class F bearings that were tested were previously deemed “non-verified” while the rest were healthy bearings and used as controls. The two Class K bearings were also used as controls and were installed on an axle on the unloaded railcar. Train speeds from 40 to 85 km/h (25 to 53 mph) were tested with the train moving at 80 km/h (50 mph) for most of the trip. The ambient air temperature fluctuated throughout the day and night, reaching as high as 33°C (91°F) during the day and as low as 6°C (43°F) during the night. Each bearing was outfitted with a custom-machined adapter that housed onboard bayonet-type (spring-loaded) thermocouples for continuous temperature measurement. The temperature data was collected using a National

Instruments™ data acquisition system. After the field-test, the temperature data from the wayside HBDs was obtained from the railroad operators for further analysis.

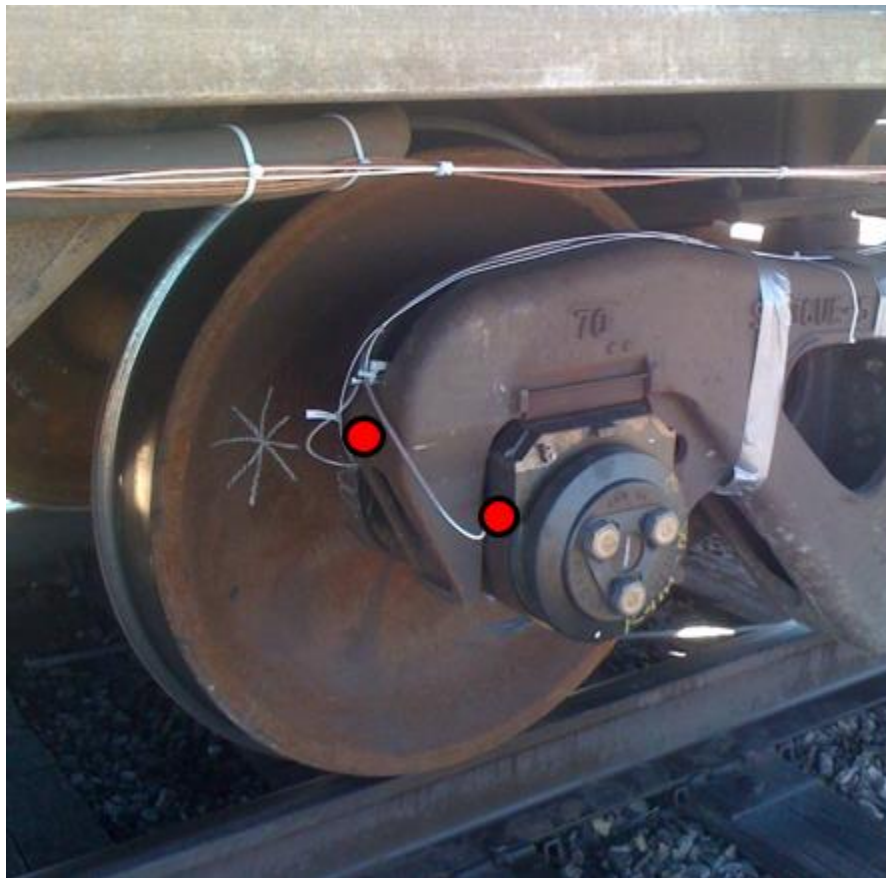


Figure 13. Field-test instrumentation setup where each red dot represents an onboard bayonet-style K-type thermocouple

3.2 Laboratory Test Setup

3.2.1 Single Bearing Test Rig

To simulate field-service wayside HBDs in a controlled environment, a single bearing dynamic test rig was designed and built by the UTCRS research team at UTRGV. The rig suspends a test bearing at one end of an axle which is driven by a motor. The tester can simulate the various speeds that a railcar may experience in the field, from 8 km/h (5 mph) to 137 km/h (85 mph). Additionally, a vertical load can be applied by a hydraulic cylinder to the bearing to

simulate loads from 10% to 150% of a fully-loaded railcar (full-load corresponds to 153 kN or 34.4 kips per bearing). Furthermore, air is circulated around the bearing using two industrial-strength fans which provide convective cooling. The latter simulates the cooling generated by the air-flow moving across the bearing as the railcar is in motion.

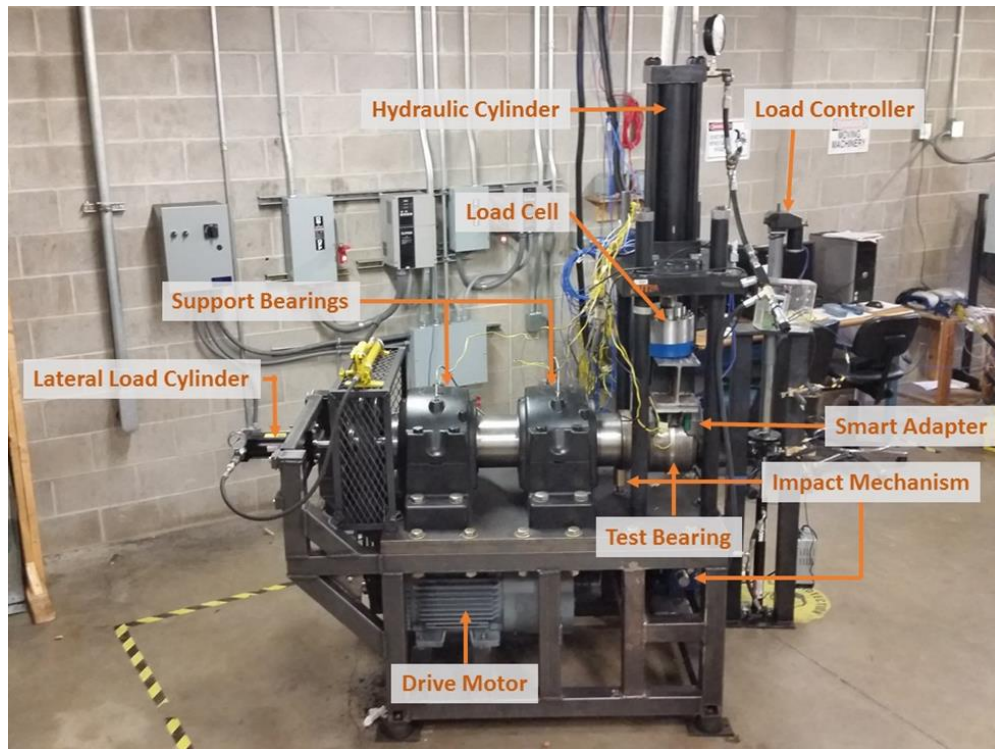


Figure 14. Single Bearing Tester (SBT) with annotations

The bearing surface temperatures along the inboard and outboard raceways were measured using four K-type spring-loaded bayonet style thermocouples. To accommodate the bayonet thermocouple holders, each bearing adapter was drilled and tapped. The bearing surface temperature was also measured using seven standard K-type thermocouples equally spaced around the circumference of the bearing at the spacer ring location.

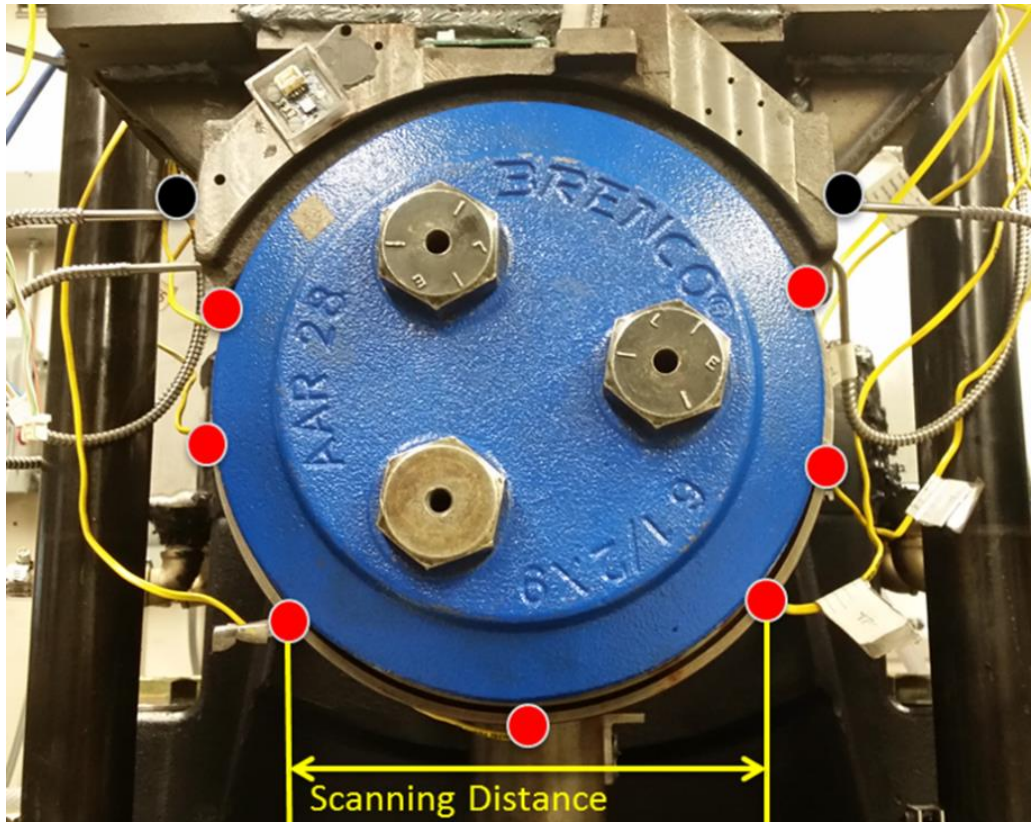


Figure 15. Bearing thermocouple locations, where each red dot represents a standard K-type thermocouple and the black dots represent spring-loaded bayonet-style K-type thermocouples

3.2.2 Laboratory Infrared Temperature Sensor

The infrared (IR) sensor that is utilized is a MICRO-EPSILON CTF-SF15-C3 miniature pyrometer. This sensor has a temperature range of -50°C (-58°F) to 975°C (1787°F) with an accuracy of $\pm 1\%$ and a resolution of less than 0.2°C (0.36°F). The sensor also has a response time of 4 milliseconds and has a spectral range of 8 to 14 micrometers. The MICRO-EPSILON sensor is utilized with a controller that provides signal processing and analog to digital conversion, which allows the sensor to be used with the associated CompactConnect software via a USB connection.



Figure 16. MICRO-EPSILON infrared (IR) temperature sensor

3.2.3 Infrared Scanning Profile

Figure 17 shows an example of the raw temperature data collected during a test. This test was performed at the 100% load setting with an axle speed simulating a train travelling at 137 km/h (85 mph). From the figure, section (1) represents the temperature measurement as the sensor passes underneath the bearing; section (2) represents the temperature measurement after it has passed underneath the bearing; and section (3) represents the temperature measurement as the sensor returns to its initial position. It should be noted that section (3) is markedly longer than section (1) because the sensor return occurs at a slower speed as it passes underneath the bearing. For each test performed in the laboratory, the temperature data in section (1) were separated and analyzed using the engineering software MATLAB™.

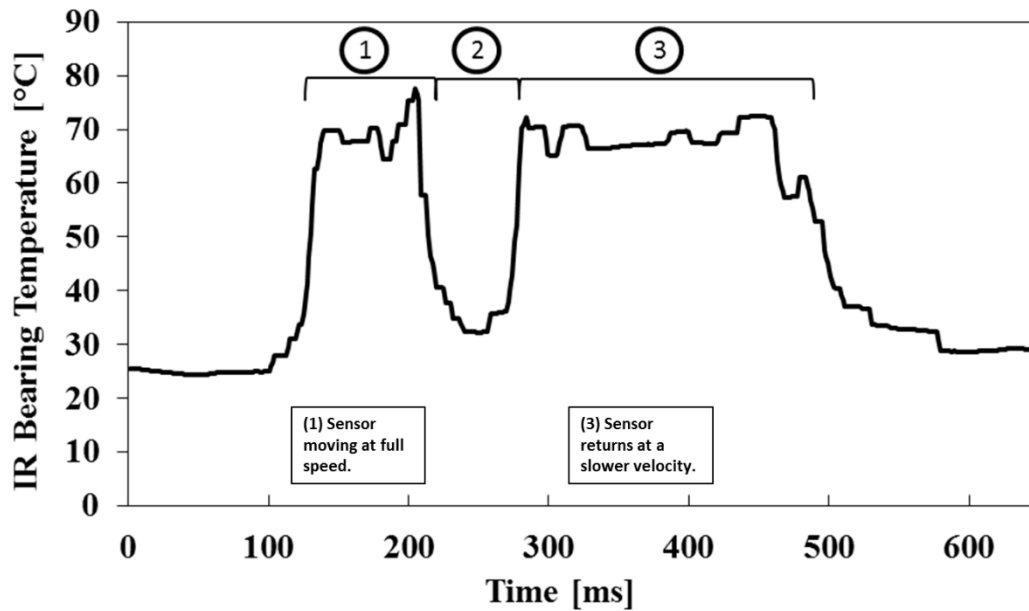


Figure 17. Typical IR sensor scanning profile

3.2.4 Test Parameters

Several parameters were varied for this study including axle speed, bearing load, bearing class, and IR scanning location. Train speeds from 48 km/h (30 mph) to 137 km/h (85 mph) were simulated in this study. A complete list of railcar speeds that were studied along with their corresponding axle speeds is given in Table 2. In addition, the bearing load was varied to simulate either an empty railcar (17% load) or a full railcar (100% load). For the 17% load setting, the load applied to the bearing was approximately 26 kN (5.85 kips) and for the 100% load setting, the load applied to the bearing was approximately 153 kN (34.4 kips). Furthermore, the cart contained a fixture that could be adjusted so that the IR sensor could scan different regions underneath the bearing. The temperature scanning regions that were studied were, as mentioned previously, the inboard (IB) seal region, the inboard raceway region, the spacer ring region, and the outboard (OB) raceway region. Over 230 tests were taken on Class K and Class F bearings traveling at the different speeds and loads described for each scanning location.

Table 2. Speeds used for test bearings in this study

Axle Speed [rpm]	Railcar Speed [mph]	Railcar Speed [km/h]
280	30	48
327	35	56
373	40	64
420	45	72
467	50	80
498	53	85
514	55	89
560	60	97
618	66	106
699	75	121
799	85	137

3.2.5 Test Bearing Conditions

For this study, a total of eleven bearings were chosen for laboratory testing based on bearing class and defect condition. Note that after the conclusion of Experiment 198C, the bearing defect grew and thus was tested again in Experiment 198D. Most bearings that were tested were Class K, while two Class F bearings were also tested. Additionally, three control bearings having no discernable defects were studied. The defective bearings in this study contained significant regions of spalling on either the bearing inner ring (cone) or bearing outer ring (cup). Cups and cones having spalls ranging in size from 4.85 cm² (0.75 in²) to 63.54 cm² (9.85 in²) were placed on either the inboard or outboard side of the bearing during testing. Figure 18 shows an example of the spalling on two of the defective bearings. Furthermore, each bearing that was tested along with its class designation, defect location, and defect area is summarized in Table 3.



Figure 18. Outer ring (cup) spall from Exp. 198C (pictured left) and inner ring (cone) spall from Exp. 202A (pictured right)

Table 3. Descriptions of the bearing laboratory testing performed for this study

Experiment Number	Bearing Class	Cone/Cup Defect	Defect Area [cm²/in²]	Defect Location
198C	K	Cup	38.14/5.91	Inboard
198D	K	Cup	63.54/9.85	Inboard
199A	K	Control	0	N/A
201B	K	Cup	28.90/4.48	Inboard
202	K	Cone	10.52/1.63	Inboard
205A	K	Cone	4.85/0.75	Inboard
206	K	Cone	38.50/5.97	Outboard
208	K	Control	0	N/A
207	K	Cone	11.39/1.77	Inboard
210	F	Control	0	N/A
217	F	Cone	8.78/1.36	Inboard

3.2.6 Data Acquisition

Infrared (IR) temperature data was acquired with the CompactConnect software that came with the IR sensor. For each test, the IR sensor was propelled underneath the test bearing a total of three times at 30-second intervals. IR temperature data was collected at a sampling rate of 1000 Hz. Additionally, continuous onboard thermocouple data was gathered with an NI cDAQ-9174 data acquisition system using an NI-9213 thermocouple input module. To collect and record the onboard thermocouple data, the engineering software LabVIEW™ was used. Average temperature measurements for each onboard thermocouple were recorded at 20-second intervals by averaging 64 samples acquired at a frequency of 128 Hz. Furthermore, the onboard thermocouple data and the IR temperature sensor data were post-processed using MATLAB™.

3.2.7 Static Testing of Infrared Sensor

To characterize the performance of the MICRO-EPSILON infrared sensor that is employed in the HBD simulator, testing was conducted in a non-dynamic environment. In this test, a bearing outer ring (cup) was placed inside a laboratory oven, where the temperature was varied from 60°C (140°F) to 120°C (248°F) at intervals of 20°C. The bearing temperature was then measured with the MICRO-EPSILON IR sensor, a non-contact IR temperature gun, and a K-type thermocouple secured tightly to the middle of the bearing cup via a hose clamp. The temperature results for all three measurement devices are presented in Table 4. The temperature measurement from the IR sensor closely matches the data collected from the IR temperature gun. However, the IR sensor temperature measurements differed from the K-type thermocouple data, with the IR sensor having an average error of 8°C (14.4°F) over the entire range of the oven test. In field service, wayside HBDs are calibrated using a one-point calibration procedure that utilizes a hot plate set to a temperature of 100°C (212°F). To ensure that the devised laboratory

HBD simulator mimics field service wayside HBDs, the data collected using the IR sensor were corrected by adding 8°C to each temperature data point to account for the one-point calibration procedure typically performed for field service wayside HBDs. Hence, any error in the temperature read by the IR sensor is due to factors other than the inherent offset error of the sensor.

Table 4. Infrared (IR) sensor oven test results [19]

Laboratory Oven Set Point [°C]	Thermocouple [°C]	IR Sensor [°C]	IR Gun [°C]
60	58	51	54
80	78	70	73
100	98	90	89
120	118	109	112



Figure 19. Oven test experimental setup [19]

3.2.8 Bearing Emissivity Values

Wayside HBDs use IR technology to scan the outer surface of the bearing cup, which may degrade over time to develop rust or other discolorations caused by environmental factors or simple heat-tinting. Consequently, one concern that needed to be resolved is the effect of this discoloration on the emissivity of the surface of bearings. Taking advantage of the numerous bearings available at UTRGV, 25 bearings with various stages of cup surface degradation, ranging from new bearings to ones that have extensive mileage in service operation and have been exposed to severe environmental factors, were selected for emissivity testing. Examples of some of the bearing surface conditions are pictured in Figure 21, which include: (1) a bearing cup that was cleaned using a pneumatic wire brush (mimics the surface conditions of a new bearing), (2) a bearing cup that has seen moderate use in service (between 250,000 and 500,000 km of operation), and (3) a bearing cup that has seen more than one million kilometers of service operation and was allowed to rust in an outdoor humid environment for three months. A forward-looking infrared (FLIR) camera was used to capture a thermal image of each bearing. By comparing the thermal image to a reference thermocouple placed on each bearing, the emissivity values of all the bearings were calculated. As seen in Table 5, it was found that the emissivity values of the bearing cup surfaces fell within a small range, with a maximum value of 0.96, a minimum value of 0.86, and a median value of 0.92. The results of this study are indicative of the population of bearings that were analyzed in this thesis. Hence, the emissivity for each bearing in this study has been assumed to be that of the median emissivity value of 0.92 [19].

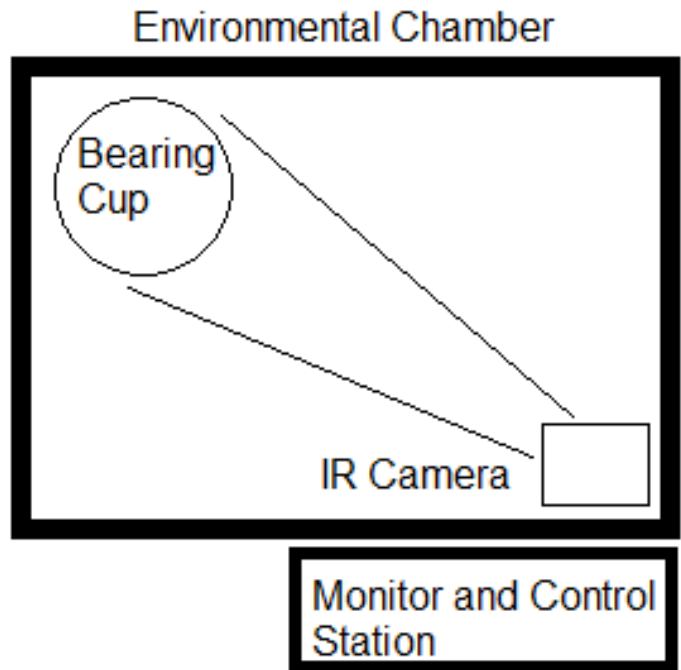


Figure 20. Overhead schematic of the setup used for bearing emissivity study. [19]



Figure 21. Examples of bearing cups used for emissivity testing includes brushed surface (left), moderately used surface (center), and heat-tinted rusted surface (right)

Table 5. Emissivity study results [19]

Bearing Outer Surface Emissivity Population Statistics	
Minimum Emissivity	0.86
Maximum Emissivity	0.96
Median Emissivity	0.92
Standard Deviation	0.02

CHAPTER IV

RADIATIVE THERMAL ANALYSIS OF RAILROAD BEARINGS

4.1 Bearing Temperature Behavior

The average operating temperatures of Class K and F bearings at various speed and load combinations are plotted in Figure 22. These operating temperatures were taken from a statistically significant population of data gathered previously by the UTCRS at UTRGV [22]. It can be observed that there is a linear increase in temperature with respect to speed for each case tested. It is also evident that increasing the load from 17% (unloaded or empty railcar) to 100% (loaded railcar) raises the operating temperature of the bearings by as much as 13°C (23°F). One important observation is that Class F and Class K bearings share a similar temperature profile at each speed and load condition. Hence, because the HBD simulation experiments in the laboratory were conducted on both Class K and Class F bearings, the temperature data acquired for these tests should be similar under the same speed and load conditions, regardless of the bearing class.

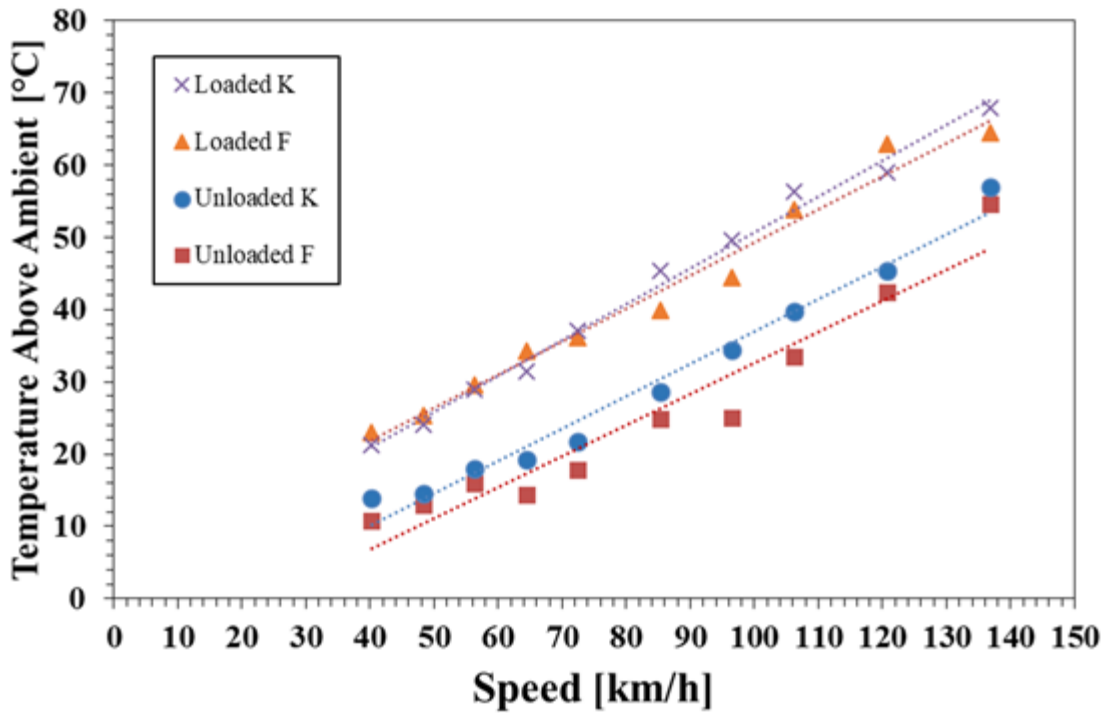


Figure 22. Class F and K bearing average operating temperatures for fully-loaded (100% load) and unloaded (17% load corresponding to empty railcar) conditions at various speeds

4.2 Bearing Temperature Profile

During service, railroad bearings are loaded on the top hemisphere of the cup while the bottom hemisphere is unloaded. Consequently, the top region of the bearing usually operates at a higher temperature compared to the bottom hemisphere of the bearing due to the better metal-to-metal contact between the rollers and the cup raceways in the top region. Figure 23 shows the temperature profile of bearings for a train travelling at 64 km/h (40 mph) and 89 km/h (55 mph) at 17% load (unloaded or empty railcar) and 100% (fully-loaded railcar). This data was acquired utilizing the single bearing tester and temperature data from the seven thermocouples and four bayonets placed around the circumference of the bearing, as shown previously in Figure 15. For empty railcar conditions, there is a gradual decrease in temperature from the top two thermocouples to the bottom three thermocouples. However, as the bearing load increases, there

is a larger contact area between the rollers and the cup in the loaded region as mentioned earlier. Hence, there is a smaller thermal resistance between these components which translates to higher temperatures in the top hemisphere of the bearing. This phenomenon is evident in Figure 23, where loading the bearing to 100% of full-load causes a noticeable increase in temperature measured by the thermocouples at the top hemisphere of the bearing as compared to the thermocouples at the bottom hemisphere.

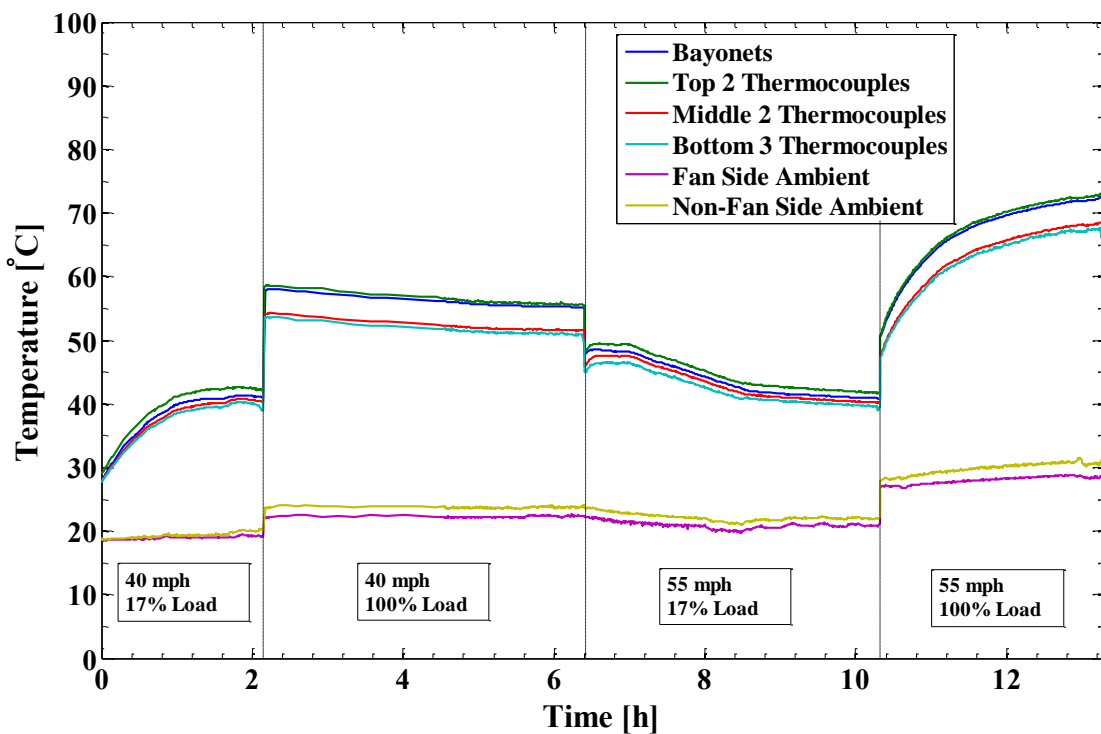


Figure 23. Bearing temperature profiles for an unloaded and loaded control bearing at 64 km/h (40 mph) and 89 km/h (55 mph)

A FLIR camera was utilized to obtain a thermal scan of the temperature profile of a Class F bearing in operation, as shown in Figure 24. This image was captured as the bearing was operating under full speed (137 km/h) and full-load (153 kN) test conditions. The thermal image

shows how the temperature of the bearing increases as it approaches the loaded region, which further validates previous observations.

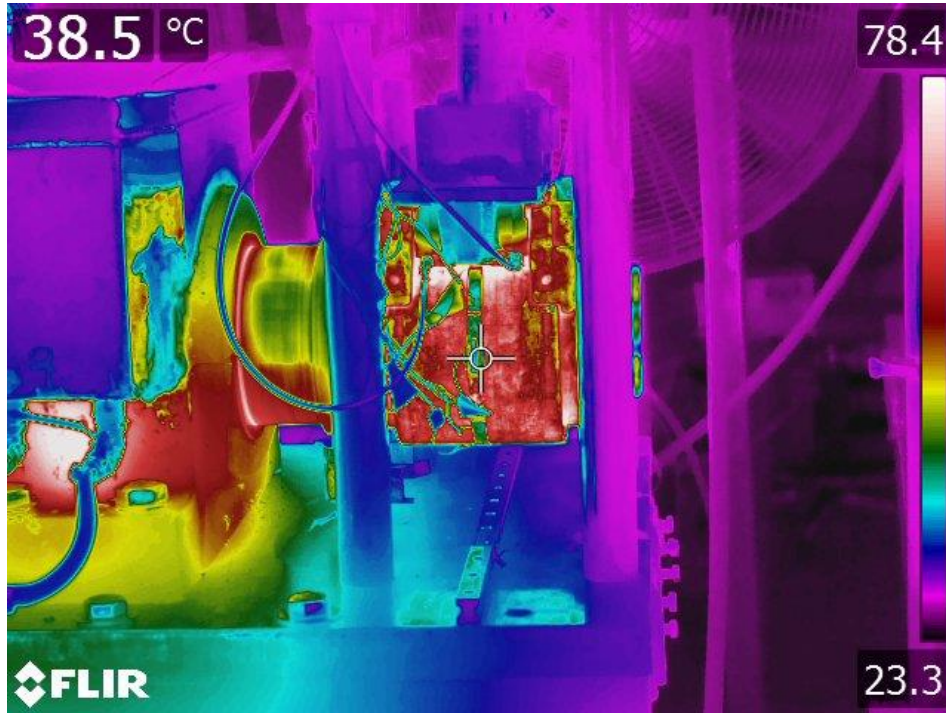


Figure 24. FLIR camera thermal image of tapered-roller bearing (side view)

From this point forward, the average of the bayonet thermocouples will be used as the most accurate bearing operating temperature. The infrared (IR) sensor data acquired utilizing the laboratory HBD simulator will be compared to the average bayonet temperatures (considered to be the true bearing operating temperature). The temperature acquired by the bayonets is a suitable predictor of the bearing temperature since the top hemisphere of the bearing experiences the maximum applied load, thus, the least thermal resistance and maximum operating temperature. Additionally, the onboard temperature data acquired in the field-test was collected using the exact same bayonet-style thermocouples mounted in a similar fashion to the onboard bayonet thermocouples used in the laboratory testing carried out for this study.

4.3 Laboratory Data Analysis

4.3.1 Raw Laboratory Data

Figure 25 through Figure 28 show the raw laboratory-acquired data utilizing the devised HBD simulator versus the onboard thermocouple data at the four scanning locations, namely: outboard raceway, spacer ring, inboard raceway, and inboard seal. The average of the two inboard bayonets was used to measure the onboard temperature for the two inboard scanning locations, the average of the two outboard bayonets was used to measure the onboard temperature for the outboard raceway scanning location, and the average of all four bayonets was used to measure the onboard temperature for the spacer ring scanning location. Note that an offset of 8°C (14.4°F) was added to all laboratory data to account for the inherent offset of the IR sensor as discussed in the Oven Test of Section 3.2.7. In each figure, the black diagonal line represents the ideal case where the HBD simulator data perfectly matches with the onboard bayonet thermocouple temperatures. Data that is shown on the left side of the line will be an overprediction of the actual bearing cup temperature, while the data on the right side of the line will be an underprediction. Upon first observation, it can be seen that the raw laboratory-acquired HBD simulator data generally underpredicts the bearing temperatures, in some cases by as much as 40°C (72°F). Furthermore, it is evident that the IR sensor error is predominantly dependent on the scanning location. For example, the outboard raceway data has greater error as compared to other scanning locations. The error band tightens as the scanning location approaches the inboard raceway region of the bearing, an observation that can be verified by examining Figure 27.

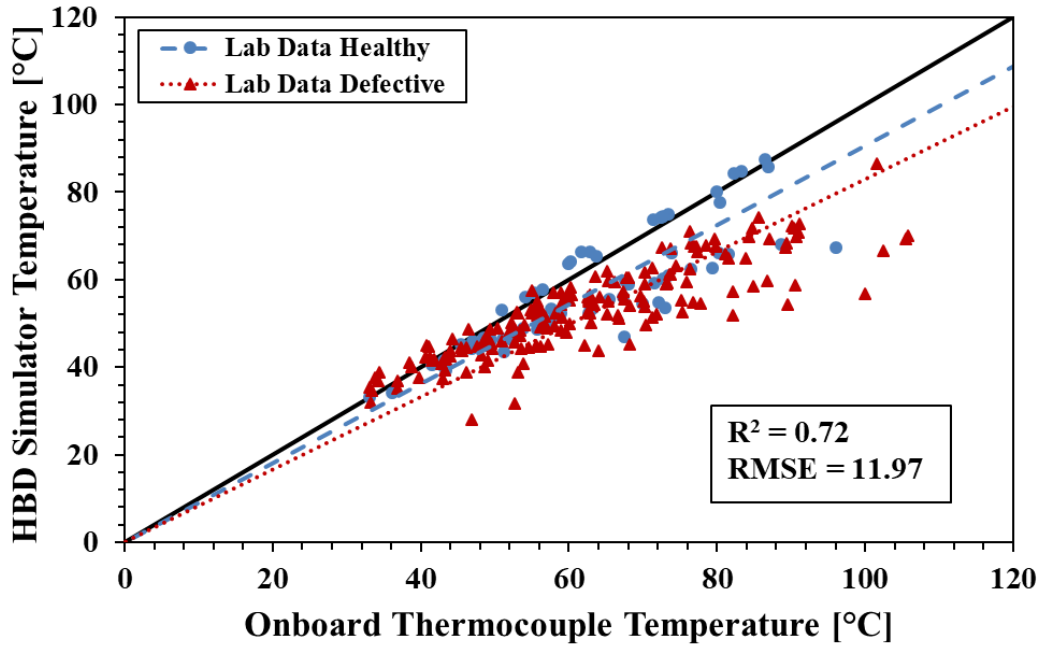


Figure 25. Laboratory raw HBD simulator temperature versus onboard bayonet thermocouple temperature for the bearing outboard (OB) raceway location

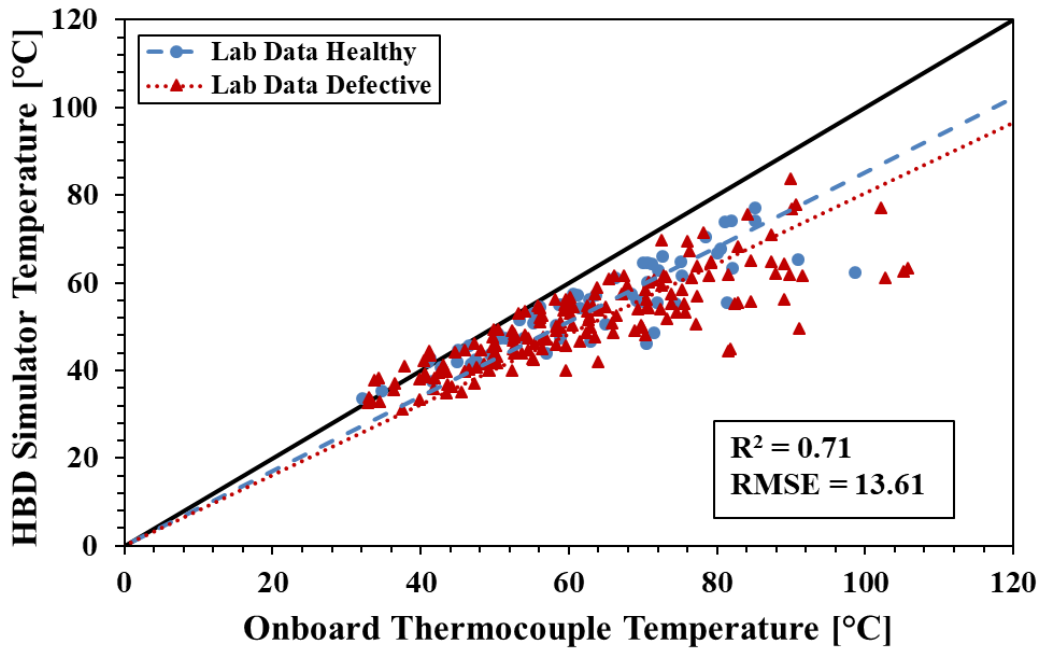


Figure 26. Laboratory raw HBD simulator temperature versus onboard bayonet thermocouple temperature for the bearing spacer ring location

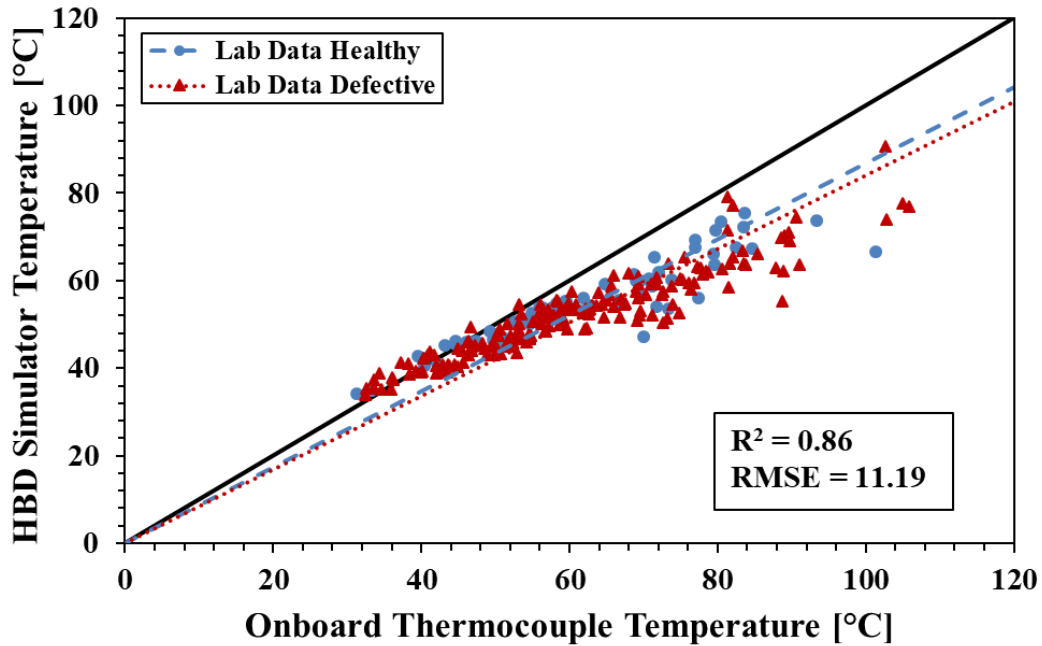


Figure 27. Laboratory raw HBD simulator temperature versus onboard bayonet thermocouple temperature for the bearing inboard (IB) raceway location

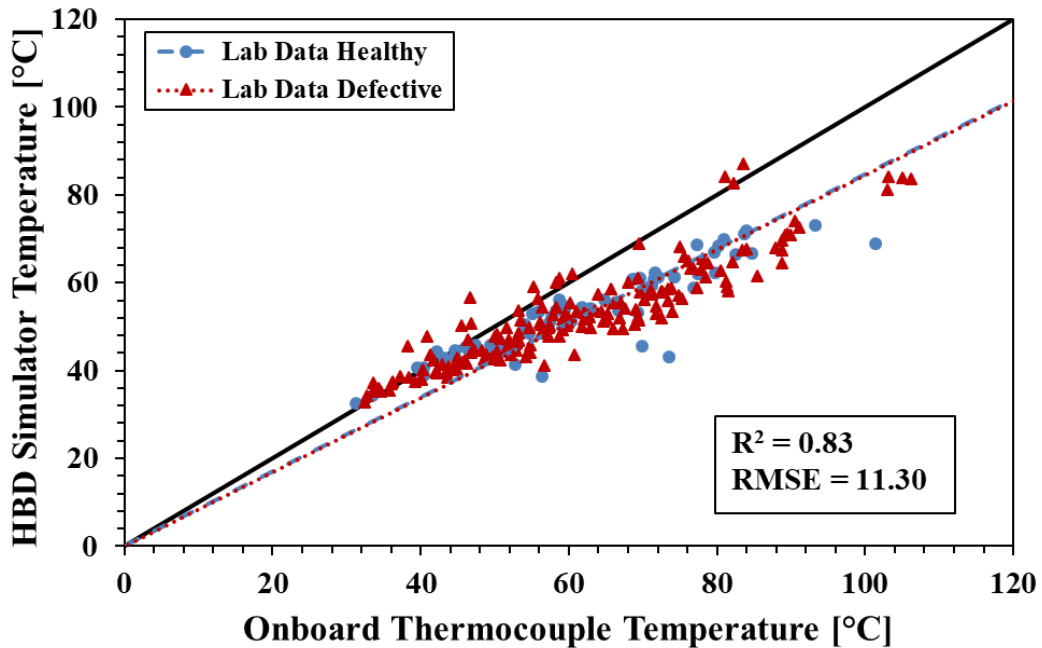


Figure 28. Laboratory raw HBD simulator temperature versus onboard bayonet thermocouple temperature for the bearing inboard (IB) seal location

4.3.2 Sensor Error Plots

A similar analysis to what is shown in Figure 29 through Figure 32 has previously been performed at the University Transportation Center for Railway Safety (UTCRS), but was incomplete due to the small data sample size. For example, the previous study analyzed only one control and one defective bearing. Since the contents of the previous study have been published [19], more data has been collected to include experiments on two more control (healthy) bearings and seven more defective bearings. The following section presents this updated data to further verify and validate previous work at the UTCRS.

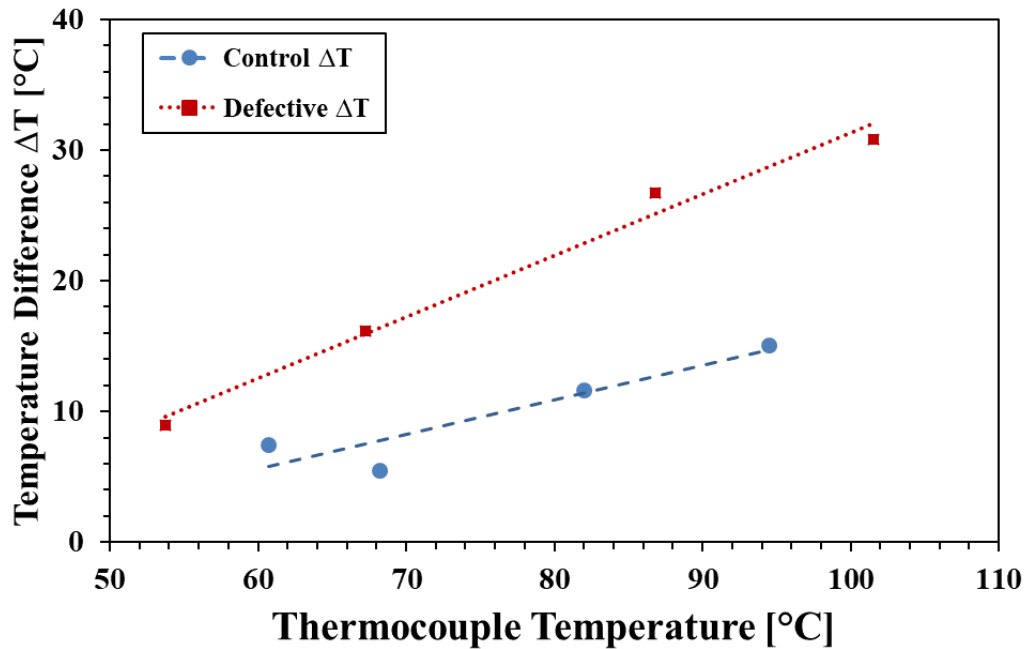


Figure 29. Infrared (IR) sensor error compared to the top two thermocouple average temperature for the outboard raceway region

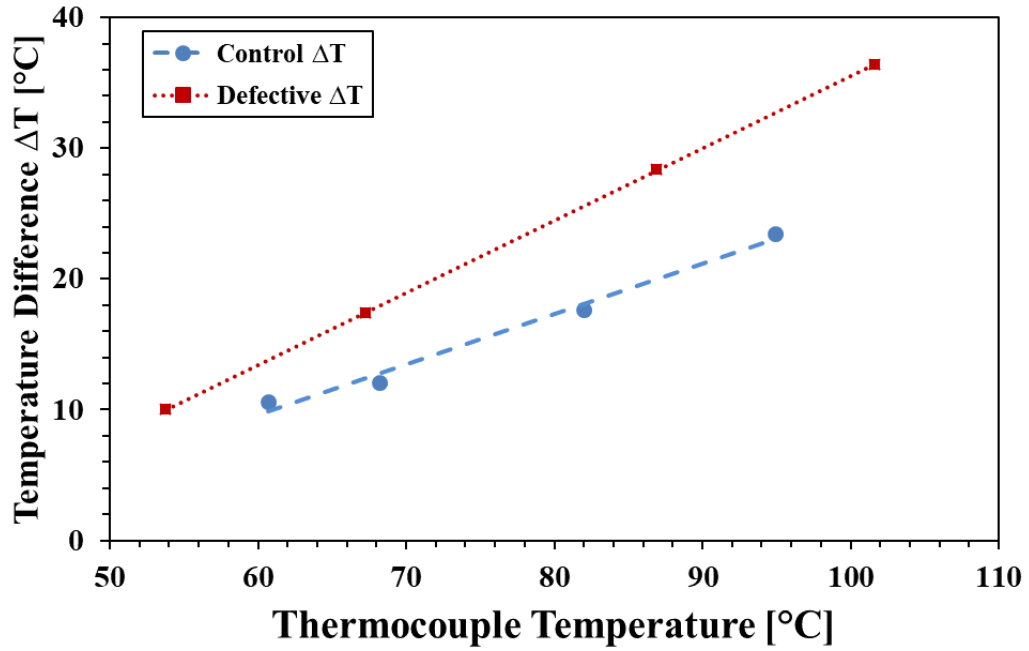


Figure 30. Infrared (IR) sensor error compared to the top two thermocouple average temperature for the spacer ring region

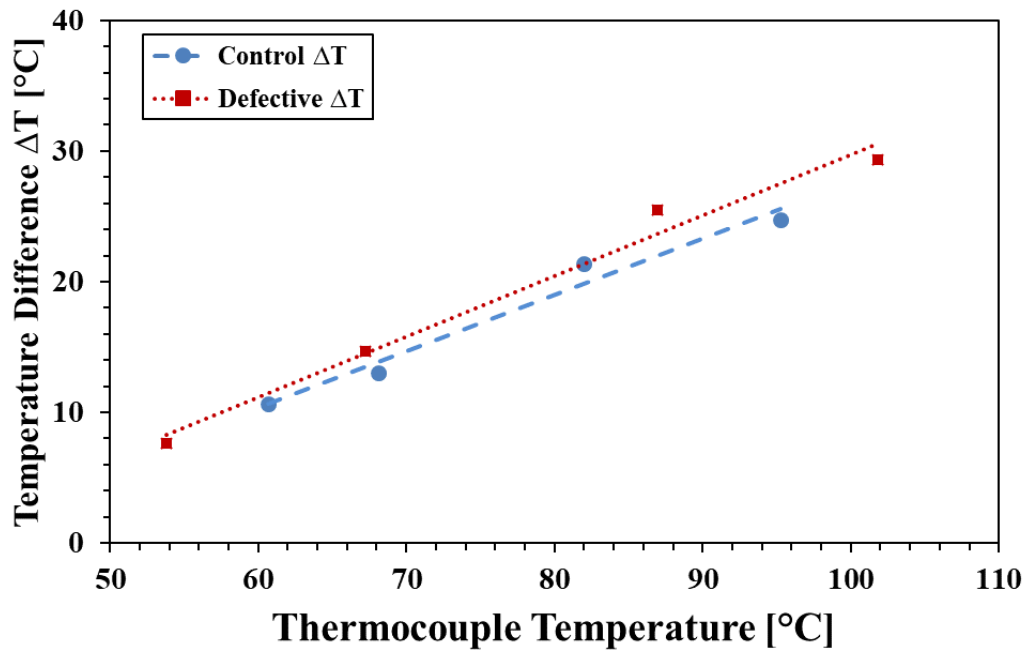


Figure 31. Infrared (IR) sensor error compared to the top two thermocouple average temperature for the inboard raceway region

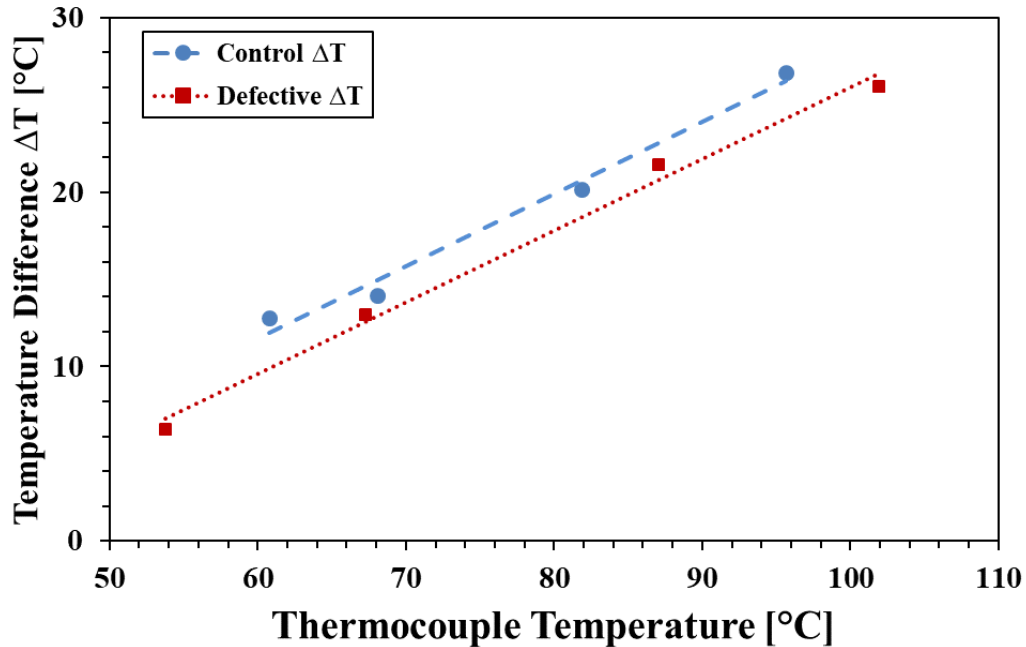


Figure 32. Infrared (IR) sensor error compared to the top two thermocouple average temperature for the inboard seal region

The infrared (IR) sensor error from the laboratory HBD simulator is analyzed in Figure 29, Figure 30, Figure 31, and Figure 32 for the outboard raceway, spacer ring, inboard raceway, and inboard seal scanning regions, respectively. These figures examine the difference in temperature between the IR sensor and the average of the top two K-type thermocouples (see Figure 15) for healthy and defective bearings. These temperature differences are averaged together and plotted against the mean bearing temperature, as measured by the top two thermocouples, at four common train speeds—48, 72, 106, and 137 km/h (30, 45, 66, and 85 mph). By examining this relationship, it is shown how the IR sensor temperature error increases linearly with the bearing operating temperature. Furthermore, this error rises at a faster rate for defective (spalled) bearings as compared to healthy (control) bearings, primarily for the outboard raceway scanning location. It is also shown that the temperatures for the defective (spalled) and healthy (control) bearings behave in the same way as the scanning location moves inward. For

example, the outboard raceway data in Figure 29 shows a significant discrepancy between the slopes of the temperature error data lines for healthy and defective bearings, but in Figure 31, the slopes of both lines are nearly identical. As mentioned in previous studies [19], this may be because the inboard seal region is not as sensitive to the effects of the spall on the bearing cup. Thus, by scanning the locations further to the bearing inboard side, it is difficult to effectively distinguish any temperature differences between healthy and defective bearings.

4.3.3 HBD Simulator Sensor Error Tables for Laboratory Testing

The sensor error tables presented in Table 6 and Table 7 were created to show the percentage of instances where the difference between the HBD simulator temperature and the onboard bayonet thermocouple temperature fell within specific temperature ranges for the four different scanning locations on the bearing. Each column in the table sums to 100%, barring any round off errors. As shown in previous sections, the HBD simulator tends to greatly underestimate the bearing temperature. In Table 7, it is shown that the temperature was underestimated by more than 17°C (31°F) around a quarter of the time for loaded bearings with a maximum underprediction of 40°C (72°F) occurring in the spacer ring scanning location. This underprediction of bearing temperature is particularly dangerous in a field setting because it may prevent a wayside HBD from predicting any overheating in bearings which could lead to catastrophic train derailments.

Table 6. Laboratory bearing temperature error for unloaded (empty railcar) bearings

ΔT [°C] (IR-TC)	OB Raceway	Spacer Ring	IB Raceway	IB Seal
	Percentage [%]			
Above 11	0	0	0	0
0 to 11	17	12	25	22
0 to -6	54	43	42	40
-6 to -11	16	27	25	25
-11 to -17	7	14	6	4
Below -17	6	4	1	8

Table 7. Laboratory bearing temperature error for loaded (full railcar) bearings

ΔT [°C] (IR-TC)	OB Raceway	Spacer Ring	IB Raceway	IB Seal
	Percentage [%]			
Above 11	0	0	0	0
0 to 11	13	1	1	7
0 to -6	13	14	21	13
-6 to -11	28	37	32	30
-11 to -17	23	21	21	27
Below -17	22	27	24	23

4.4 Field Test Data Analysis

4.4.1 Raw Field Test Data

The raw field-acquired wayside HBD data is shown in Figure 33. Note that the typical scanning location for wayside HBDs in field service is similar to what was indicated in Figure 5 in Section 1.3. After examining the raw field data, it is evident that the wayside HBD in the field generally underpredicted bearing temperatures, in some cases by as much as 47.2°C (85°F). This underestimation of bearing temperature is dangerous and may prevent the wayside HBD from reporting any problematic bearings that are overheating. Conversely, the wayside HBD overpredicted the bearing temperature in many cases, reaching an error of almost 25°C (45°F). Overpredicted bearing temperatures such as this can result in false trending events that may cause unnecessary and costly train stoppages and delays. This wide range of temperature error may be attributed to the lack of precision in the HBD measurements, which is evident from the scatter that the temperature data exhibits.

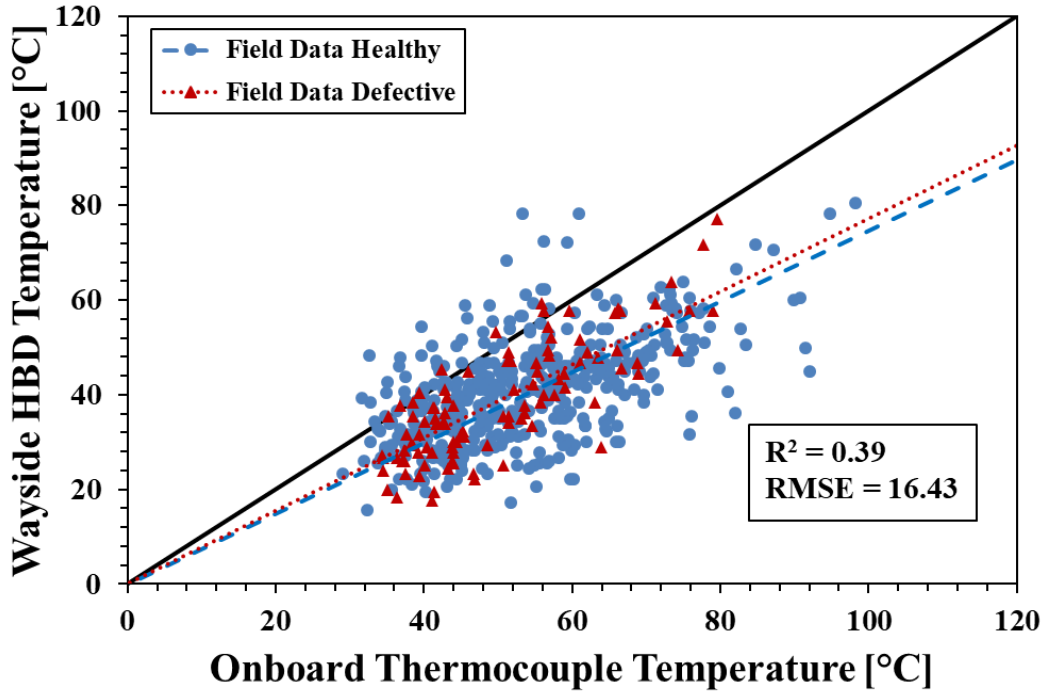


Figure 33. Raw field-test wayside HBD temperature versus onboard thermocouple temperature

4.4.2 HBD Sensor Error Tables for Field Testing

Table 8 summarizes the temperature difference between the onboard bayonet and the wayside HBD temperatures categorized under several temperature ranges. The table separates the field-test data by bearing class and load condition. For unloaded Class K bearings, the wayside HBDs overpredict the bearing temperature 35% of the time; 7% of the time the temperature difference is greater than 11°C (20°F) and 28% of the time the temperature difference is between 0°C (0°F) and 11°C (20°F). For unloaded Class F bearings, the HBDs overpredict the bearing temperature only 10% of the time. In conclusion, the wayside HBDs are more likely to overpredict Class K bearing temperatures as compared to Class F bearings under the same conditions, thus, suggesting that there is an inherent bias in the HBDs in relation to bearing class. Furthermore, after examining loaded Class F bearings, it is evident that the HBDs underpredict these temperatures around 95% of the time. In fact, the HBDs underpredicted all

bearing temperatures by more than 17°C (31°F) more than one-third of the time. Once again, any underprediction of bearing temperatures is troubling because the HBD system will fail to detect and report any problematic bearings, which may result in catastrophic derailments.

Table 8. Raw field-test bearing temperature error

ΔT [°C] (IR-TC)	Class K Unloaded	Class F Unloaded	Class F Loaded	Total
Percentage [%]				
Above 11	7	0	1	1
0 to 11	28	10	4	9
0 to -6	12	18	8	12
-6 to -11	22	29	20	24
-11 to -17	12	18	22	19
Below -17	19	26	46	35

CHAPTER V

HOT BOX DETECTOR (HBD) OPTIMIZATION

It is common practice that HBDs are calibrated in an industry setting to produce the most accurate results possible. This process often involves relying on a linear calibration applied by the manufacturer of the HBD infrared (IR) sensor or applying a one-point calibration to the HBD using a hot plate with a known temperature to remove any offset error. Nevertheless, as presented in Section 4.4, wayside HBDs tend to generally underpredict the bearing operating temperatures and, in some cases, grossly overpredict the bearing operating temperatures. These results have shown that the calibration methods that are commonly performed in the industry are ineffective, particularly because the simple calibration methods fail to account for the largest sources of error in the HBD, which are: (1) the dynamic response of the sensor and (2) the temperature difference between the bottom and top of the bearing during service operation. In this chapter, the data that was collected and presented in Chapter IV will be used to explore different calibration methods to optimize the data recorded by the HBD simulator in the laboratory and the data acquired during the service field-test.

5.1 Laboratory Data Optimization

5.1.1 Calibration Methods

Multiple calibration equations were created to optimize the data collected by the HBD simulator. Since it was found that more precise HBD temperature measurements are taken closer to the inboard side of the bearing, the following three calibrations use dynamic infrared (IR)

temperature data taken at the inboard raceway scanning location. This data was calibrated against the average of the two inboard bayonet thermocouples. For the two-point and three-point calibrations, given in Figure 34, the calibration points were chosen by selecting laboratory HBD simulator readings that were closest to their corresponding bayonet thermocouple measurements. In the case of the two-point calibration, the lowest temperature reading recorded by the IR sensor that matched (within $\pm 3^{\circ}\text{C}$) the average bayonet thermocouple temperature was chosen as one of the points, whereas, the second point chosen was the highest IR sensor reading that matched (within $\pm 3^{\circ}\text{C}$) the average bayonet thermocouple temperature. For the three-point calibration, an intermediate third point was chosen between the lowest and highest temperatures recorded following the same criteria used to choose the other two points. The third calibration that was performed on the laboratory data is presented in Figure 35. This calibration was performed utilizing all of the inboard raceway temperature data acquired in the laboratory as calibration points.

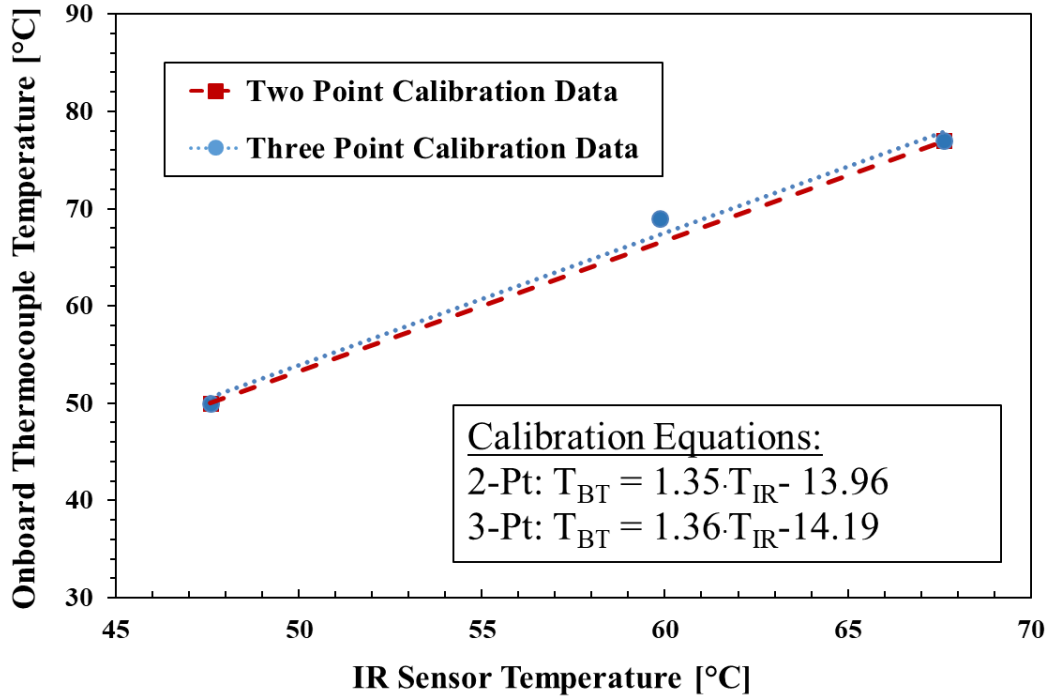


Figure 34. Two-point and three-point calibrations using data acquired by the laboratory HBD simulator

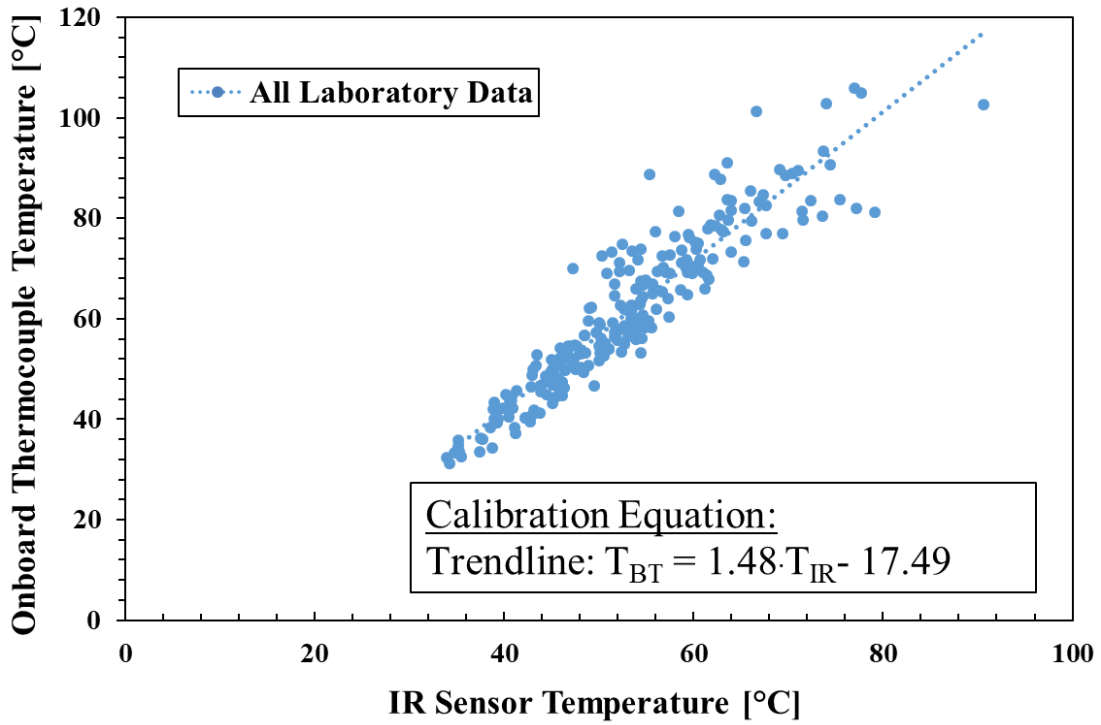


Figure 35. Calibration using the trendline through all data collected by the laboratory HBD simulator

5.1.2 Coefficient of Determination and Root-Mean-Squared Error

Table 9 provides the root-mean-square-error (RMSE) and the coefficient of determination (R^2) values for the temperature measurements obtained by the HBD laboratory simulator. Figure 36 and Figure 37 summarize the RMSE and R^2 for all the data that was acquired, both for loaded and unloaded operation conditions, using the HBD simulator. The data was divided by load condition and scanning location. The RMSE is defined as:

$$RMSE = \sqrt{\frac{\sum(T_{IR} - T_{expected})^2}{n}} \quad (1)$$

In Equation (1), T_{IR} represents the temperature measured by the infrared (IR) sensor or wayside HBD, while $T_{expected}$ is the actual temperature of the bearing, which in this case is the average value of the onboard bayonet thermocouple temperatures. Additionally, n is defined as the number of data points obtained. The RMSE is dependent on the square of the error, placing more “weight” on outliers. As such, the RMSE will be used as a measure of the accuracy of the IR sensor temperature measurement, with lower RMSE values corresponding to more accurate measurements. Furthermore, the coefficient of determination (R^2) is a numerically determined value that represents how well the dataset fits a regression line. Holding the accuracy of the measurement independent, the coefficient of determination will be used to quantify the precision of the dataset.

Table 9. Coefficient of determination (R^2) and root-mean-squared-error (RMSE) for various calibrations

Data Description		RMSE [$^{\circ}$ C]				R^2
		Raw Data	2-Pt. Cal.	3-Pt. Cal.	All-Data Cal.	
Unloaded	OB Raceway	7.27	5.94	5.85	6.37	0.81
	Spacer	8.09	6.48	6.20	5.76	0.81
	IB Raceway	5.99	3.59	3.46	4.09	0.92
	IB Seal	7.70	5.83	5.59	5.26	0.82
Loaded	OB Raceway	14.37	11.04	10.78	10.53	0.57
	Spacer	16.41	12.72	12.29	10.88	0.55
	IB Raceway	13.70	8.80	8.31	6.81	0.78
	IB Seal	13.25	8.81	8.41	7.53	0.76
All Laboratory Data	OB Raceway	11.97	9.28	9.08	9.04	0.72
	Spacer	13.61	10.61	10.24	9.12	0.71
	IB Raceway	11.19	7.13	6.75	5.84	0.86
	IB Seal	11.30	7.73	7.38	6.69	0.83

It is evident that the RMSE value improves as the scanning location moves inboard, as indicated by the decreasing RMSE, regardless of the calibration method chosen. The results show that scanning the inboard (IB) raceway location yields the most accurate results for both load conditions. Additionally, the R^2 value improved as the scanning location approached the inboard raceway region of the bearing, demonstrating that the temperature measurements are the most precise at this scanning location as well. These observations agree with the conclusions from the TTCI study [15]. Furthermore, applying the calibrations significantly improved the performance of the laboratory HBD simulator. For fully-loaded bearings, adding more calibration points significantly improved the accuracy of the data in each scanning location. For example, by calibrating the raw data using the two-point calibration, the RMSE for loaded bearings scanned at the inboard (IB) raceway location improved from 13.70 $^{\circ}$ C (24.66 $^{\circ}$ F) to 8.80 $^{\circ}$ C (15.84 $^{\circ}$ F). By adding another calibration point to create the three-point calibration, the RMSE improved to 8.31 $^{\circ}$ C (14.96 $^{\circ}$ F). By using all of the laboratory-acquired data to calibrate

the HBD simulator, the RMSE was lowered even further to 6.81°C (12.26°F). Although the RMSE for unloaded bearings marginally increased when the all-data calibration was applied, the RMSE of all HBD simulator data, for both unloaded and loaded, decreased markedly indicating that the temperature data has been optimized. Note that applying a calibration to the data did not change the R^2 value of the dataset, implying that the precision of the data cannot be corrected using these calibration methods. However, this analysis demonstrates that adding more data points to a calibration can significantly improve the accuracy of wayside HBDs.

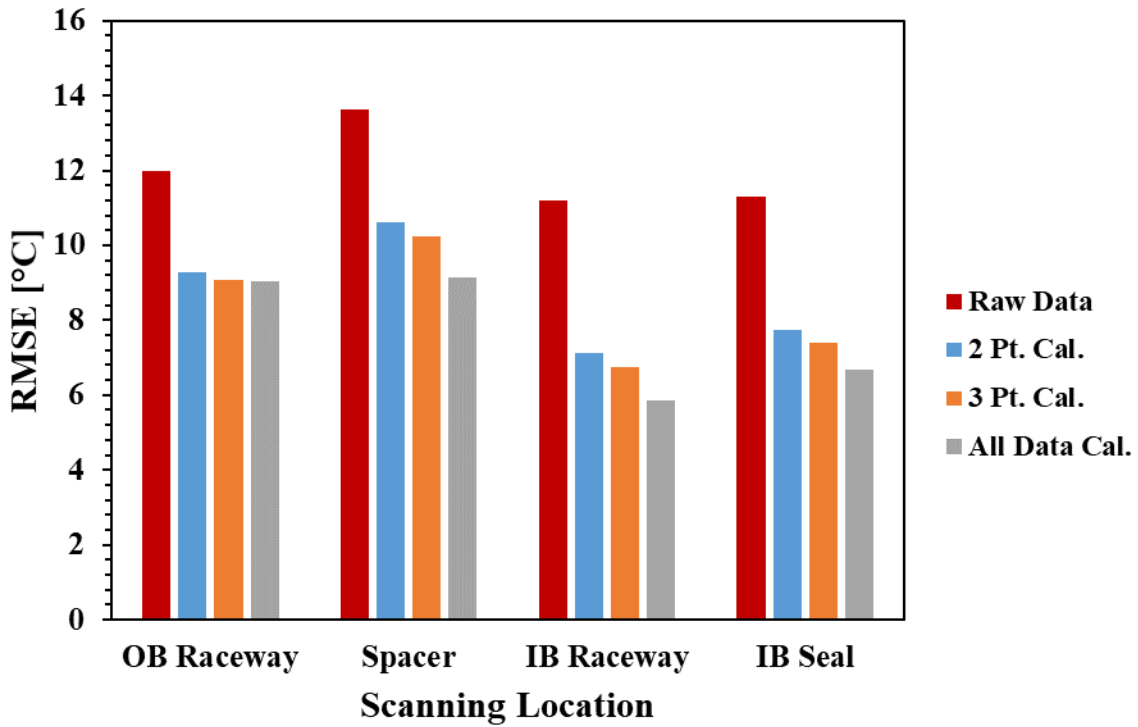


Figure 36. All laboratory data root-mean-squared-error (RMSE) comparison for various calibrations at each scanning location

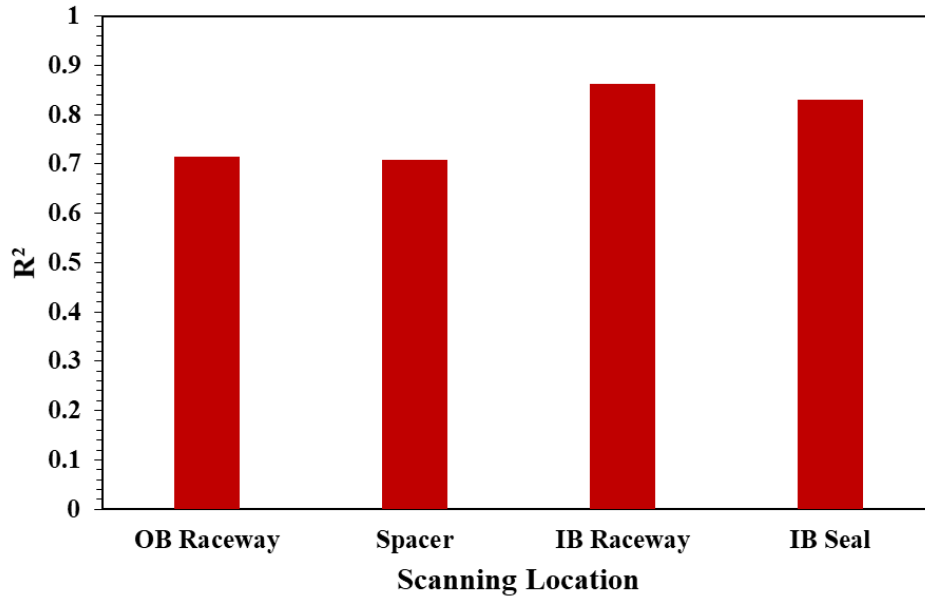


Figure 37. All laboratory data coefficient of determination (R^2) for various calibrations at each scanning location

5.1.3 Calibrated Laboratory HBD Simulator Data

Figure 38 through Figure 41 show the HBD simulator data versus the onboard bayonet thermocouple temperature data acquired from laboratory testing. Once again, the infrared (IR) temperature data was recorded at four different scanning locations: outboard (OB) raceway, spacer ring, inboard (IB) raceway, and inboard seal. The solid diagonal line in each figure represents an ideal relationship where the HBD simulator and the onboard thermocouple data are perfectly matched. Accordingly, the temperature data that is overpredicted by the IR sensor will be present on the left side of the line while the data that is underpredicted by the IR sensor will be present on the right side of the line. Lastly, each dataset was divided into two categories, healthy and defective bearings.

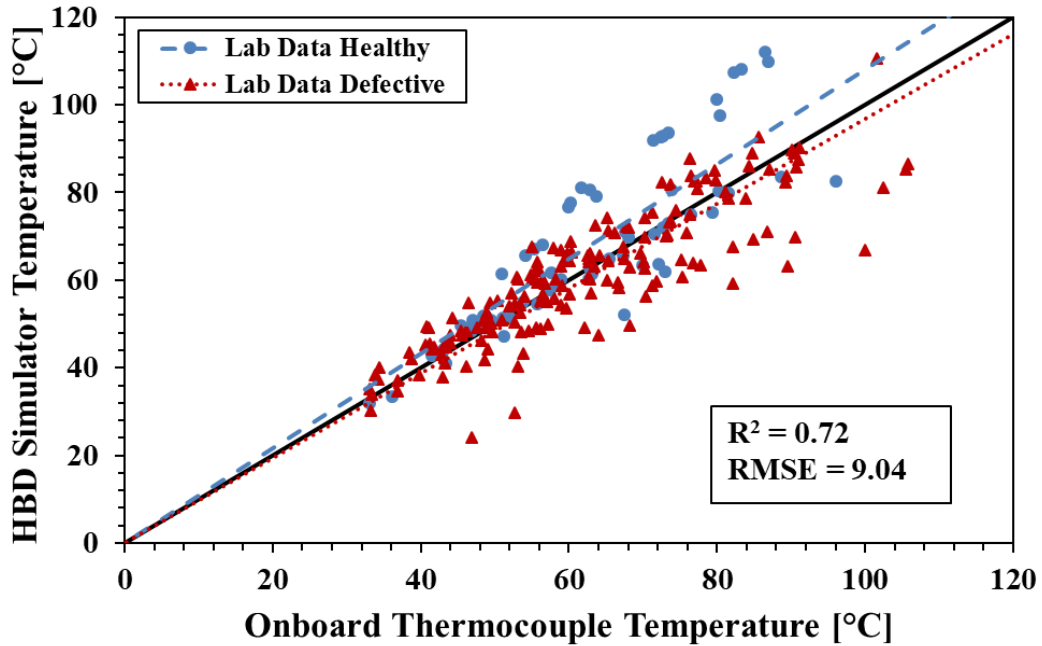


Figure 38. Calibrated laboratory HBD simulator temperature versus onboard bayonet thermocouple temperature for the bearing outboard (OB) raceway location

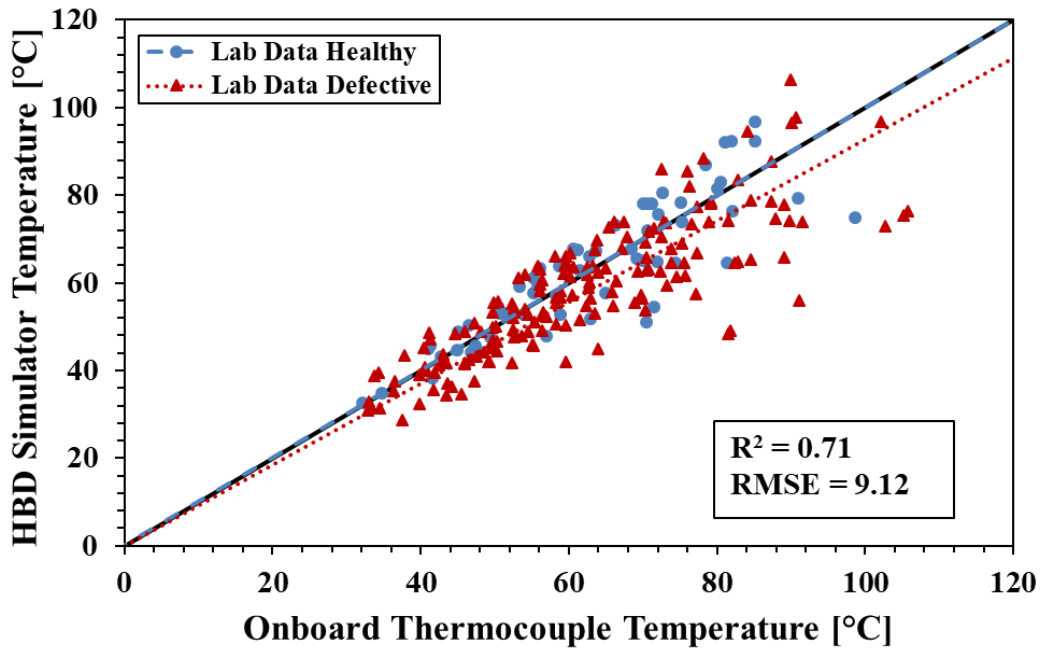


Figure 39. Calibrated laboratory HBD simulator temperature versus onboard bayonet thermocouple temperature for the bearing spacer ring location

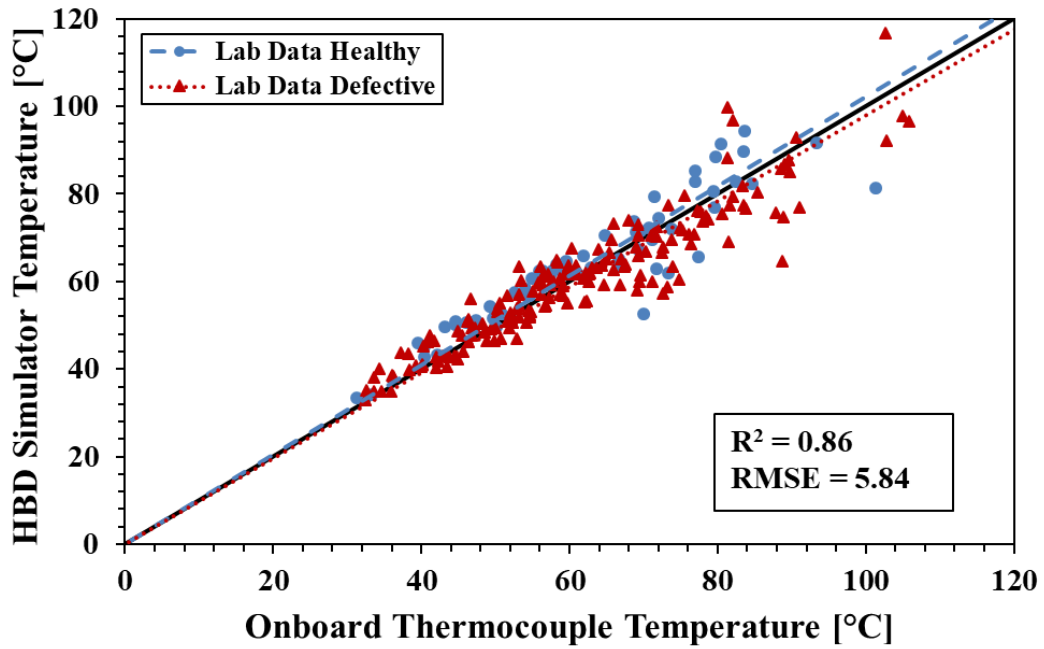


Figure 40. Calibrated laboratory HBD simulator temperature versus onboard bayonet thermocouple temperature for the bearing inboard (IB) raceway location

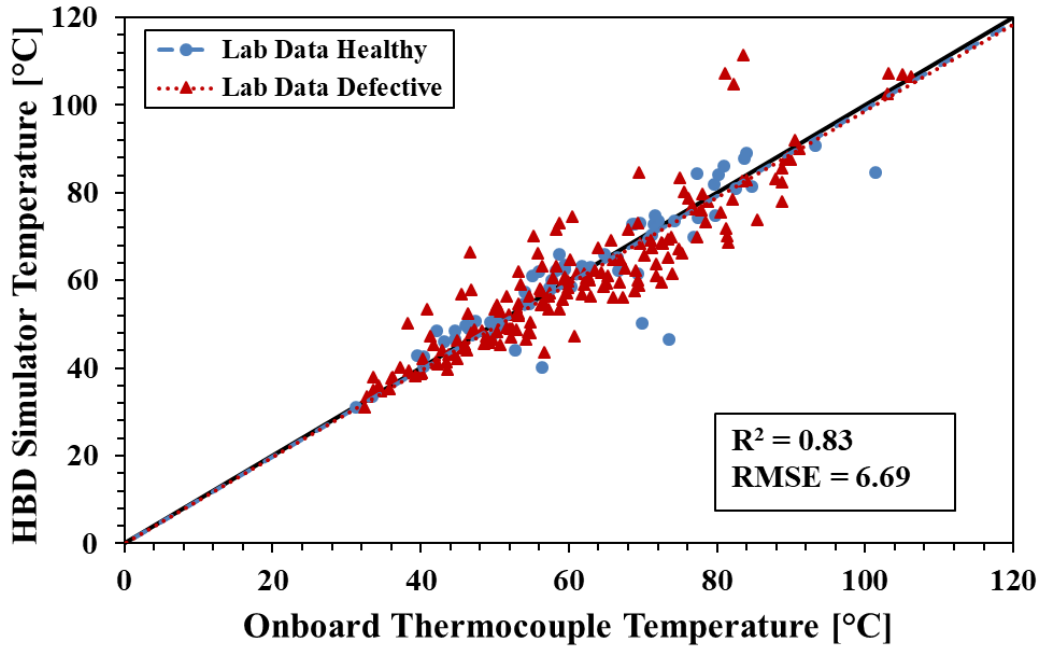


Figure 41. Calibrated laboratory HBD simulator temperature versus onboard bayonet thermocouple temperature for the bearing inboard (IB) seal location

After examining the calibrated laboratory-acquired data, it is evident that the temperature error between the HBD simulator and the onboard thermocouples is dependent on the scanning location. Out of the four scanning locations, the temperatures measured by the outboard raceway location have the most variance, also indicated by its low R^2 value of 0.72. The data acquired in this scanning location tends to overpredict the bearing temperature by as much as 25°C (45°F) and underpredict the bearing temperature by almost 33°C (59.4°F), in some cases. It is also apparent that as the scanning location moves from the outboard raceway to the inboard raceway, the temperature error decreases, as can be seen in Figure 40. Finally, one important finding is that the laboratory HBD simulator, after the calibration is applied, tends to predict higher temperatures for healthy bearings as compared to defective bearings. This observation is troubling considering that defective bearings may deteriorate rapidly leading to disastrous consequences.

Table 10. Laboratory bearing temperature error for unloaded (empty railcar) bearings

ΔT [°C] (IR-TC)	OB Raceway	Spacer Ring	IB Raceway	IB Seal
	Percentage [%]			
Above 11	3	1	0	4
0 to 11	68	44	73	52
0 to -6	18	35	24	35
-6 to -11	5	17	3	4
-11 to -17	3	2	0	5
Below -17	2	1	0	0

Table 11. Laboratory bearing temperature error for loaded (full railcar) bearings

ΔT [°C] (IR-TC)	OB Raceway	Spacer Ring	IB Raceway	IB Seal
	Percentage [%]			
Above 11	13	1	2	7
0 to 11	30	39	37	31
0 to -6	33	19	41	43
-6 to -11	10	19	10	14
-11 to -17	9	8	7	3
Below -17	5	13	2	2

Table 10 and Table 11 show the percentages of instances where the temperature difference between the HBD simulator data and the onboard bayonet thermocouples fell within six prescribed temperature ranges. These tables categorize the data according to bearing load condition. Once again, each column in the table sums to 100%, barring any round-off errors. Table 10 shows that, in the case of unloaded bearings, the inboard (IB) raceway scanning location temperature error (ΔT) fell consistently in the range between -11°C (-20°F) and 11°C (20°F) for every single temperature measurement. For all loaded bearings scanned in the IB raceway location, the majority ($\sim 88\%$) of temperature measurements fell within the same range, as indicated in Table 11. As the infrared (IR) scanning location moves further outboard, however, it is evident that more bearing temperature readings fall into less acceptable ranges. For example, for loaded bearings scanned in the outboard (OB) raceway region, 14% of temperature measurements underpredict the bearing operating temperature by more than 11°C (20°F), while 13% of temperature measurements overpredict the bearing temperature by more than 11°C (20°F). These results are important in freight rail service because overpredicted temperature measurements can lead to healthy bearings being removed from service and underpredicted temperatures may lead to defective and problematic bearings being left in service. Hence, it is crucial that wayside HBDs in field service are set to scan the inboard (IB) raceway region of the bearing cup to obtain the most reliable and accurate bearing operating temperature.

5.1.4 Other Calibration Methods

In addition to the dynamic two-point calibration that was performed in Section 5.1.1, two more calibration methods were explored, as shown in Figure 42, by placing the infrared (IR) sensor underneath the bearing and recording IR temperature data for one minute at two different

speed and load combinations. Because the IR sensor is static for these calibrations and there is no error due to the dynamic response of the sensor, these calibrations will be referred to as “Static Calibrations.” During these calibrations, the bearing experienced a simulated speed of 97 km/h (60 mph) with a 17% load condition (empty railcar) for the cool calibration temperature and 100% load (full railcar) for the hot calibration temperature. For the static calibration (TC), the IR sensor temperature is compared to the bottom thermocouple, which is generally affected by the vibration of the rotating bearing. For the static calibration (BT), the IR sensor is compared to the onboard bayonet thermocouples (i.e., average temperature of the four bayonet thermocouples), which takes into account the temperature difference between the bottom and top of the bearing. The “Final Calibration” in Figure 42 is the two-point calibration presented in Section 5.1.1, which accounts for the dynamic response of the IR sensor utilizing the laboratory HBD simulator.

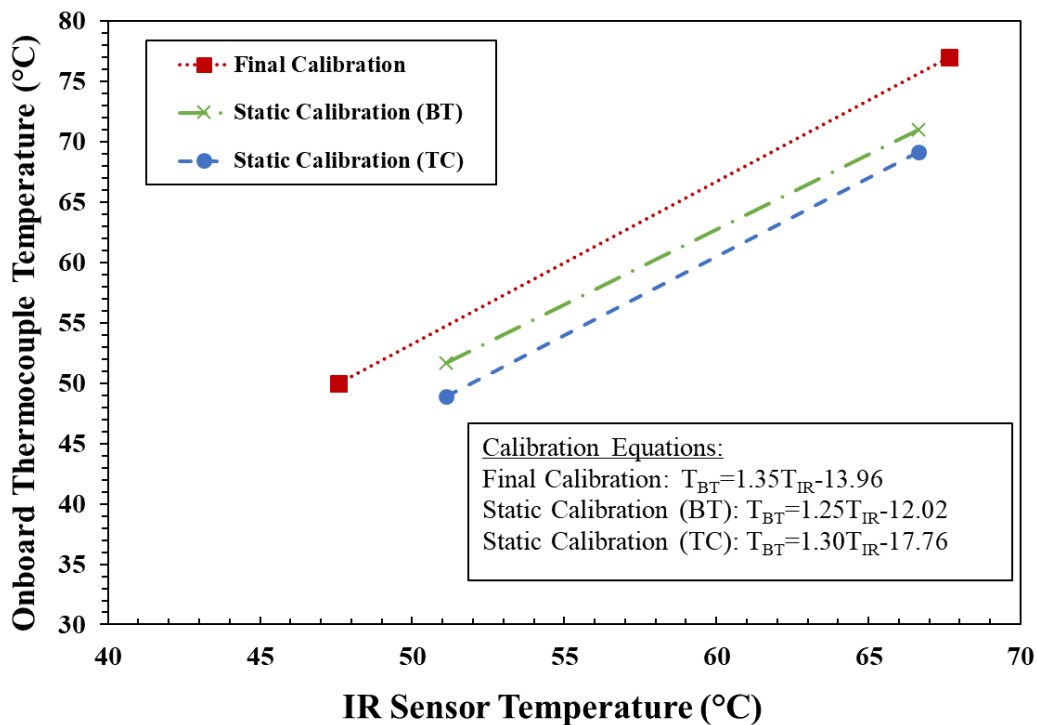


Figure 42. Various two-point calibrations for laboratory-acquired data

Table 12 shows the root-mean-squared error (RMSE) for laboratory HBD simulator data after each of the calibrations given in Figure 42 were applied. Alternatively, a bar graph which summarizes the results of the calibrations is provided in Figure 43. By moving the static calibration from the bottom thermocouple to the bayonet thermocouples, the RMSE decreases significantly for all cases tested, which shows that the temperature difference between the bottom and top of the bearing is a significant source of error. Additionally, by accounting for the dynamic response of the IR sensor in the final calibration, the IR sensor temperature error is lowered even further. Hence, this calibration procedure was chosen as the optimal two-point calibration because it accounts for the largest sources of error in the system, which are: (1) the dynamic response of the system and (2) the temperature difference between the bottom and top of the bearing. It should be noted that the optimal calibration method uses the trendline through all data acquired by the HBD simulator, as given in Section 5.1.1.

Table 12. Coefficient of determination (R^2) and root-mean-squared-error (RMSE) for other calibrations explored in this study

Data Description		RMSE [$^{\circ}$ C]			R^2
		Static Cal. (TC)	Static Cal. (BT)	Final 2-pt Cal.	
Unloaded	OB Raceway	9.29	7.13	5.94	0.81
	Spacer	10.69	8.21	6.48	0.81
	IB Raceway	7.63	5.29	3.59	0.92
	IB Seal	9.87	7.53	5.83	0.82
Loaded	OB Raceway	14.74	12.94	11.04	0.57
	Spacer	17.24	15.16	12.72	0.55
	IB Raceway	13.67	11.65	8.80	0.78
	IB Seal	13.37	11.37	8.81	0.76
All Laboratory Data	OB Raceway	12.79	10.93	9.28	0.72
	Spacer	14.92	12.77	10.61	0.71
	IB Raceway	11.58	9.56	7.13	0.86
	IB Seal	12.07	9.98	7.73	0.83

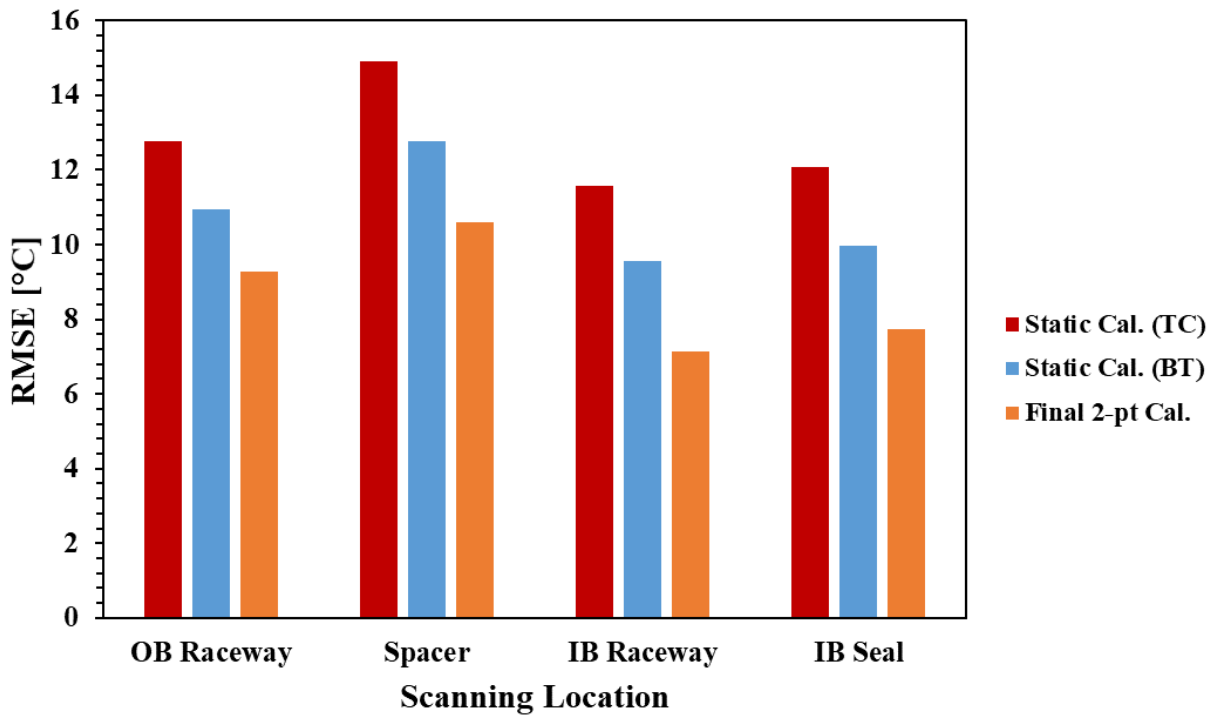


Figure 43. Root-mean-squared-error (RMSE) for other two-point calibration methods that were explored for this study

5.2 Field Data Optimization

5.2.1 Calibration Methods

A similar calibration procedure to that used for the laboratory-acquired data was applied to the field-test data. The two-point and three-point calibrations using the field-test data are provided in Figure 44. For both of these calibrations, the calibration points are chosen by selecting the wayside HBD temperature readings that are closest to their corresponding average bayonet thermocouple measurements. For consistency, the calibration temperatures are acquired only from Class K bearings. Additionally, another calibration was devised using the trendline through all field-acquired data (including Class K and F), as presented in Figure 45.

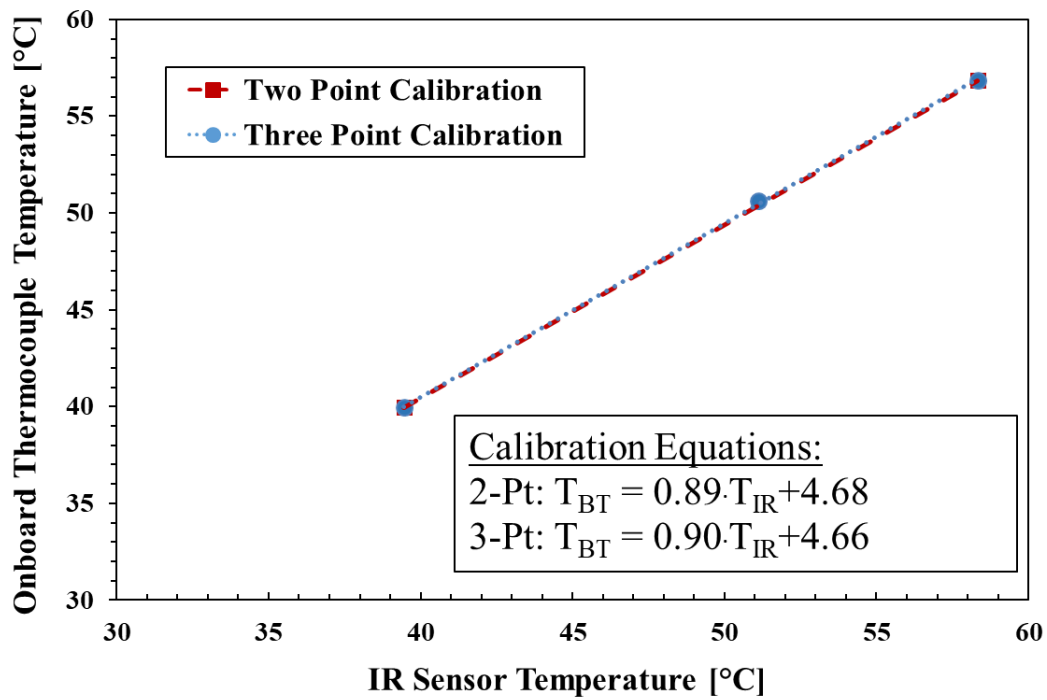


Figure 44. Two-point and three-point calibrations using field-test data

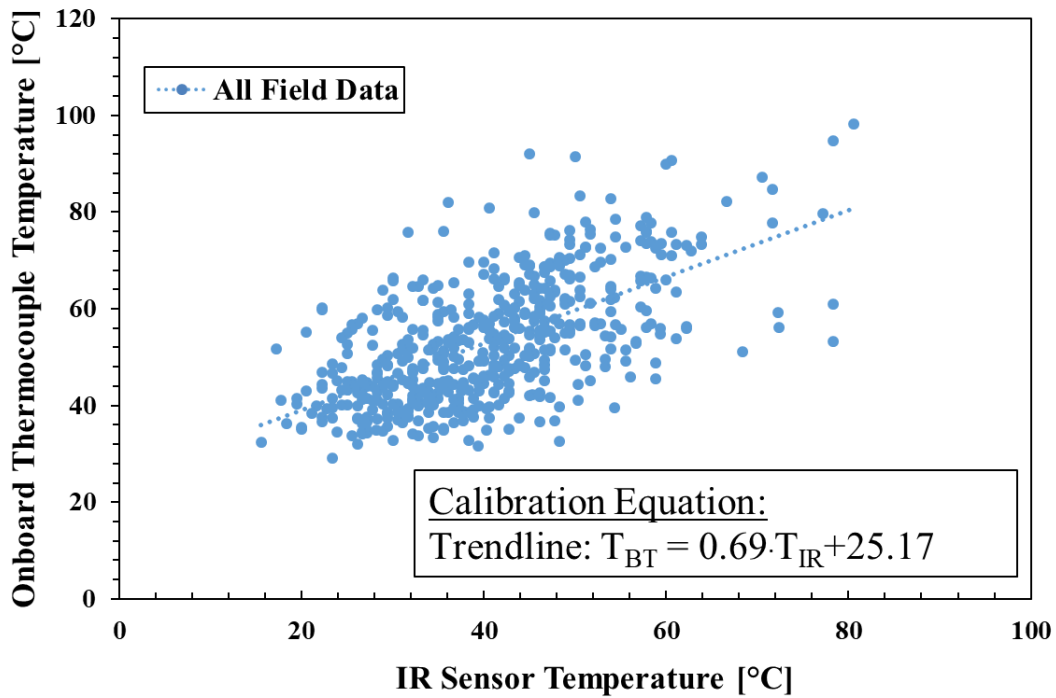


Figure 45. Calibration equation using the trendline through all data collected during the in-service field test

5.2.2 Coefficient of Determination and Root-Mean-Squared Error

Table 13, Figure 46, and Figure 47 provide the coefficient of determination (R^2) and the root-mean-squared-error (RMSE) for the field-test data. Table 13 sorts the data based on load condition and bearing class. It is evident that the field-acquired data is less precise and less accurate than the laboratory-acquired data (given in Table 9) as indicated by the smaller R^2 value and greater RMSE value, respectively. Furthermore, the loaded Class F bearing temperature measurements appear to be less accurate but more precise than temperature measurements taken for unloaded Class F bearings. Moreover, the unloaded Class K bearing temperature measurements are more accurate but less precise than both the unloaded and loaded Class F data for the two-point and three-point calibrations. However, for the all-data calibration, the unloaded Class K data is less accurate and less precise than the unloaded and loaded Class F data.

Table 13. Coefficient of determination (R^2) and root-mean-squared-error (RMSE) for various calibrations utilized

Data Description	RMSE [$^{\circ}\text{C}$]				R^2
	Raw Data	2-Pt. Cal.	3-Pt. Cal.	All Data Cal.	
Unloaded Class F	14.35	13.26	13.49	8.52	0.17
Loaded Class F	18.56	18.32	18.28	10.41	0.46
Unloaded Class K	12.73	12.20	12.32	11.67	0.13
Unloaded and Loaded Class F	16.9	16.39	15.99	9.67	0.45
Unloaded Class K and F	13.95	13.00	13.2	9.43	0.19
All Class K and F	16.43	15.92	15.57	9.94	0.39

By examining the results before and after the calibrations were applied, it can be observed that the accuracy of the data improved substantially when the all-data calibration method was implemented. After applying the two-point calibration to the data, the root-mean-squared-error (RMSE) decreased minimally from 16.43°C (29.57°F) to 15.92°C (28.66°F). Adding another calibration point has negligible effect on the RMSE which decreases slightly from 15.92°C (28.66°F) to 15.57°C (28.03°F). The latter observation is expected, given that the two-point and three-point calibration equations listed in Figure 44 are almost identical. The linear calibration using all field-acquired data yielded the most accurate results with an RMSE value of 9.94°C (17.89°F). Finally, it should be noted that the coefficient of determination (R^2) value does not change by applying the different calibrations, indicating that the precision of the measurements cannot be improved using a linear calibration procedure.

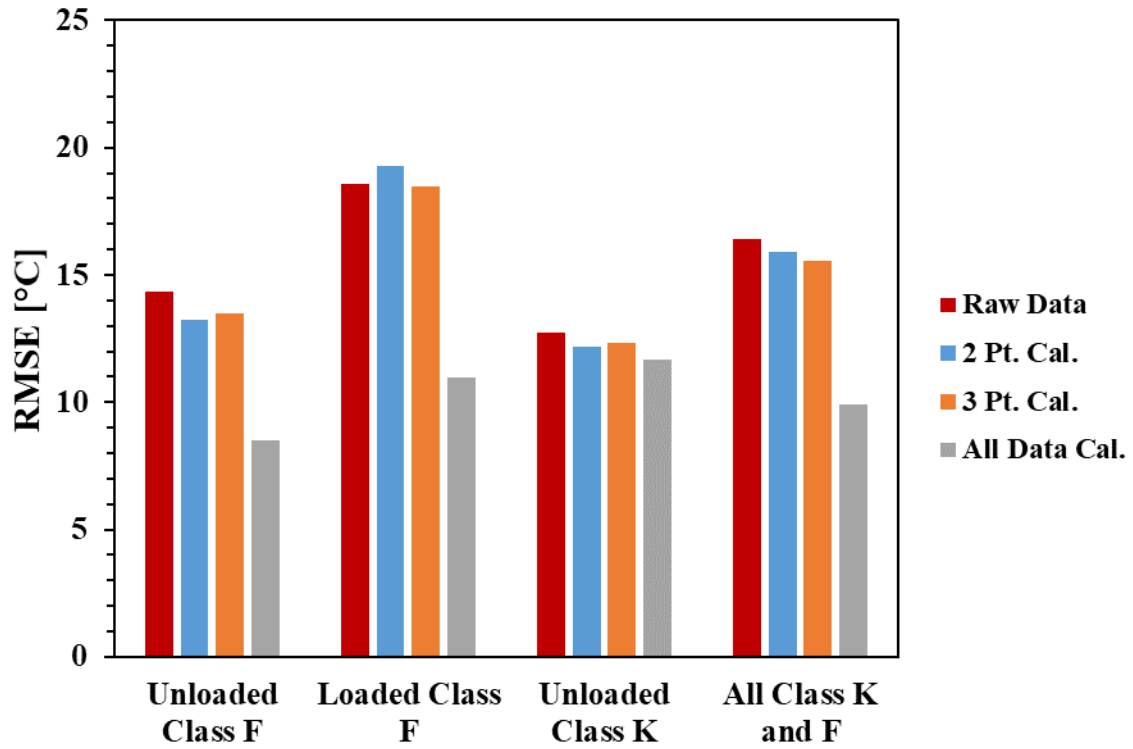


Figure 46. Root-mean-squared-error (RMSE) comparison for all test cases in the field test



Figure 47. Coefficient of determination (R^2) comparison for all test cases in the field test

5.2.3 Calibrated Field Service HBD Data

The effect of the calibration using the trendline through all field-acquired data points on the wayside HBD data is presented in Figure 48. This calibration method was selected because it yielded the most accurate results. It is evident in Figure 48 that the applied calibration significantly improves the wayside HBD temperature data as compared to the raw data presented in Figure 33. However, there are still instances where the wayside HBD readings overpredict bearing temperatures by as much as 26°C (47°F) and underpredict bearing temperatures by almost 35°C (63°F). The latter is due to the inability of the linear calibration to correct the precision in the wayside HBD temperature measurements. Nonetheless, applying this calibration method significantly improves the accuracy of the wayside HBD temperature data.

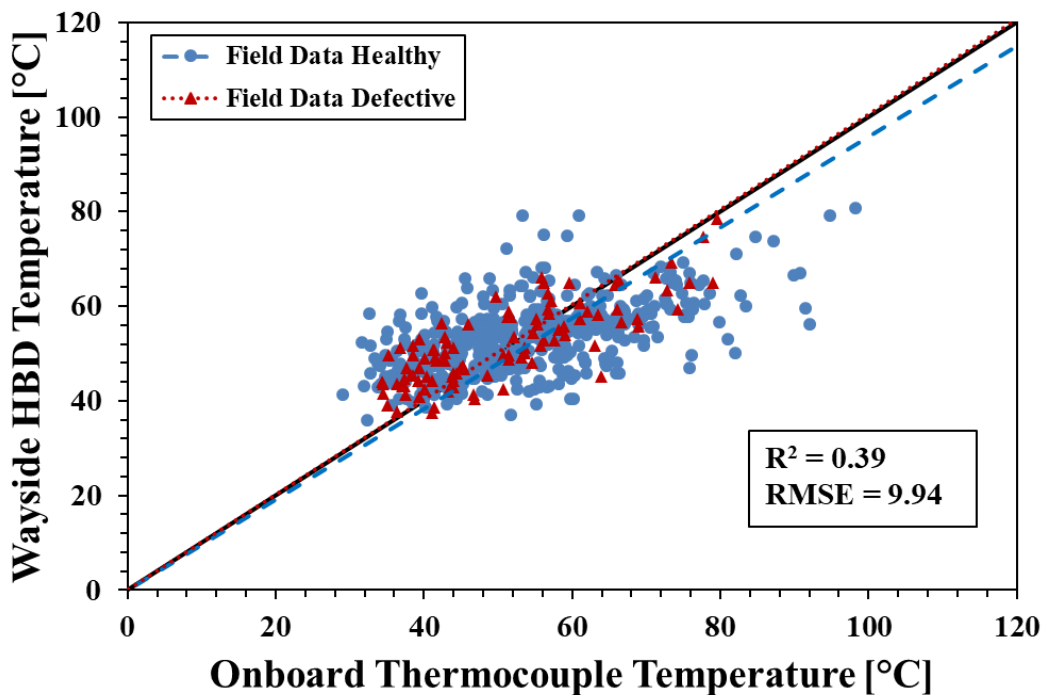


Figure 48. Calibrated field-test wayside HBD temperature versus onboard thermocouple temperature

Further analysis of the calibration using all data acquired during the field-test can be examined in Table 14. From the distribution of percentages in the sensor error table, it is evident that the inherent bias with respect to temperature measurements between Class K and Class F bearings was not corrected by applying the calibration method. Furthermore, the percentage of instances where the temperature error fell between -11°C (-20°F) and 11°C (20°F) for all bearings increased from 45%, as given in Table 8, to 73%, as listed in Table 14, which shows that applying the calibration improved the wayside HBD data significantly. However, the wayside HBDs still overpredict the temperature of the bearings by more than 11°C (20°F) almost 12% of the time with a maximum overprediction of 25.8°C (46.5°F), which may be a potential cause for false setouts of otherwise healthy bearings.

Table 14. Calibrated field-test bearing temperature error

ΔT [°C] (IR-TC)	Class K Unloaded	Class F Unloaded	Class F Loaded	Total
	Percentage [%]			
Above 11	34	15	5	12
0 to 11	37	57	29	40
0 to -6	16	17	26	21
-6 to -11	4	4	19	12
-11 to -17	9	6	13	10
Below -17	0	2	9	5

CHAPTER VI

CONCLUSIONS AND RECCOMENDATIONS

An investigation into the efficacy of wayside HBDs that are currently used in rail service was conducted. The laboratory HBD simulator was fabricated to mimic the functionality of the wayside HBDs in field service by traversing an infrared (IR) sensor underneath a bearing to take a dynamic temperature measurement. Numerous experiments were performed in the laboratory using healthy and defective bearings at various speed and load conditions. The data was analyzed and then subsequently compared with the data acquired during an on-track field service test.

Analysis of the results has led to many important conclusions. It was found that field service HBDs are greatly affected by the bearing class due to the fact that the change in bearing dimensions between bearing classes causes the IR sensor to scan different regions of the bearing outer ring (cup). In order to verify this observation, laboratory data was acquired at different scanning locations on the bearing. In the laboratory, it was concluded that the scanning location on the bearing significantly affects the temperature measurement of the laboratory HBD simulator, with the most accurate and precise results coming from the inboard raceway region of the bearing cup. These observations are important because incorrect bearing temperature measurements can lead to unnecessary train stoppages or, in some cases, costly derailments.

Generally, wayside HBDs tend to underestimate the temperatures of bearings in field service operation, which is not surprising given the simple one-point calibration procedure that is used to calibrate these devices. This temperature underprediction can have disastrous

consequences, especially if a defective bearing goes undetected by a wayside HBD. This scenario has occurred on numerous occasions in the past two decades in the U.S. and Canada. Hence, an optimized calibration technique along with proper IR sensor alignment can markedly improve the accuracy and precision of HBD temperature measurements, which in turn, can reduce: (a) costly delays and train stoppages associated with false warm bearing trending events, and (b) catastrophic bearing failures associated with HBDs underestimating the operating temperature of a defective bearing. This study explored different calibration techniques and applied them to the data that was acquired in the laboratory and from a specially planned field test. It was found that using more calibration points significantly improved the accuracy of wayside HBD temperature measurements, while having no effect on the precision.

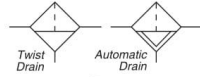
The shortcomings of wayside HBD systems are prevalent and not readily correctable. An alternate method to monitor bearing condition continuously and reliably would be preferred. One such system could be implemented using advanced onboard monitoring technologies, which is currently a focus of study at the University of Texas Rio Grande Valley (UTRGV). In this system, the bearing operating temperature is directly measured at the loaded region of the bearing and is collected continuously. Additionally, incorporation of accelerometers into this system will facilitate a more in-depth bearing condition monitoring and analysis that will allow the early detection of the onset of bearing failure so that the bearing can be tracked and removed from service operation before it deteriorates to the point where it can lead to a catastrophic bearing failure that results in costly train derailments.

APPENDIX A

APPENDIX A

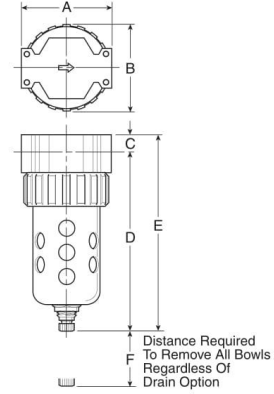
WAYSIDE SIMULATION COMPONENT SPECIFICATION

07F Filters – Standard



Features

- Excellent water removal efficiency.
- Unique deflector plate and shroud creates a swirling of the air stream ensuring maximum water and dirt separation.
- Large filter element surface guarantees low pressure drop and increased element life.
- Optional automatic float drain available.
- Shown with recommended metal bowl guard.
- High Flow: 1/2" – 130 SCFM[§]
 3/4" – 145 SCFM[§]



Distance Required To Remove All Bowls Regardless Of Drain Option

Port Size	NPT	
	Twist Drain	Automatic Float Drain
Poly Bowl† / Metal Guard		
1/2"	07F32AC	07F36AC
3/4"	07F42AC	07F46AC
Metal Bowl / Sight Gauge		
1/2"	07F34AC	07F38AC
3/4"	07F44AC	07F48AC

07F Filter Dimensions		
A 3.24 (82)	B 3.25 (83)	C .70 (18)
D 6.97 (177)	D† 7.00 (178)	E 7.67 (195)
E† 7.70 (196)	F 2.75 (70)	

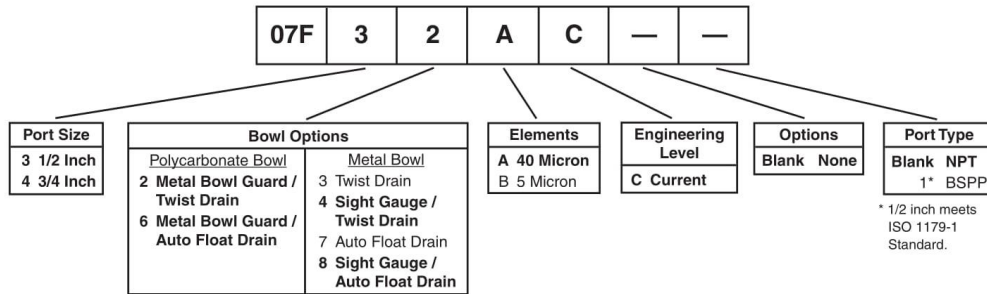
Inches (mm)
 † With Automatic Float Drain

Standard part numbers shown bold.
 For other models refer to ordering information below.

† For polycarbonate bowl see Caution on page C2.

§ SCFM = Standard cubic feet per minute at 90 psig inlet and 5 psig pressure drop.

Ordering Information



BOLD ITEMS ARE MOST POPULAR.

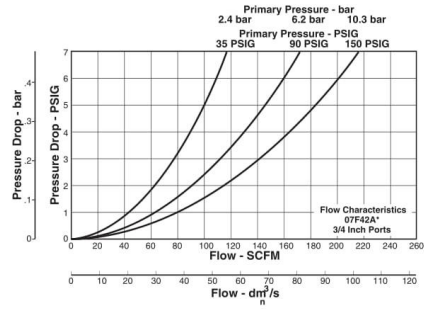
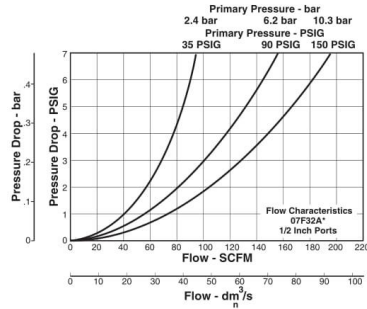


C20

Parker Hannifin Corporation
 Pneumatic Division
 Richland, Michigan
 www.parker.com/pneumatics

Technical Specifications – 07F

Technical Information



07F Filter Kits & Accessories

Bowl Guard Kit	PS805P
Bowl Kits –	
Poly Bowl –	
Automatic Float Drain	PS822P
Twist Drain	PS832P
Metal Bowl –	
Automatic Float Drain	PS826P
Twist Drain	PS834P
Sight Gauge / Automatic Drain	PS823P
Sight Gauge / Twist Drain	PS835P
DPI Replacement Kit	PS781P
Drain Kits –	
Automatic Float Drain	PS506P
Semi-Auto Drain	PS511P
Twist Drain	PS512P
Push 'N' Drain	PS513P
Filter Element Kits –	
40 Micron	PS801P
5 Micron	PS802P
Adsorber	PS831P
Mounting Bracket Kit	PS843P
Sight Gauge Kit	PS914P
Specifications	
Bowl Capacity	7.2 Ounces
Sump Capacity	2.8 Ounces
Port Threads	1/2, 3/4 Inch

Pressure & Temperature Ratings –

Without Differential Pressure Indicator:	
Polycarbonate Bowl – 0 to 150 psig (0 to 10.3 bar)	32°F to 125°F (0°C to 52°C)
Metal Bowl – 0 to 250 psig (0 to 17.2 bar)	32°F to 175°F (0°C to 80°C)
With Differential Pressure Indicator:	
0 to 150 psig (0 to 10.3 bar)	32°F to 125°F (0°C to 52°C)
Automatic Float Drain – 15 to 250 psig (1.0 to 17.2 bar)	
Weight	2.2 lb. (1.0 kg)

Materials of Construction

Body	Zinc
Bowls	Transparent Polycarbonate
	Metal (Zinc) With or Without Sight Gauge
Bowl Guards	Steel
Collar	Plastic or Metal
Deflector, Shroud & Baffle	Plastic
Drains –	
Twist Drain – Body & Nut	Plastic
Push 'N' Drain –	
Body	Nitrile
Stem	Brass
Automatic Float Drain –	
Housing, Float	Plastic
Seals	Nitrile
Springs, Push Rod	Stainless Steel
Filter Elements –	
40 Micron (Standard)	Plastic
5 Micron (Optional)	Plastic
Adsorber (Optional)	Activated Charcoal
Seals	Nitrile
Sight Gauge	Polyamide



C

Product Selection

Filters

Coalescers

Regulators

Filter / Regulators

Lubricators

Combs

Accessories

Air Line Lubricators

Prep-Air II Air Preparation Units

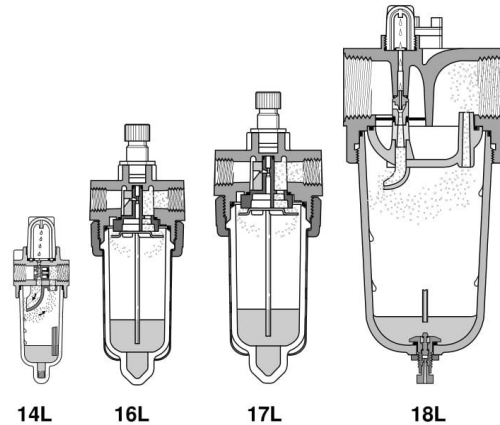
Micro-Mist Lubricators

- Pipe Sizes 1/4 thru 1-1/2 Inch
- Flows to 500 SCFM
- Pressures to 250 PSIG



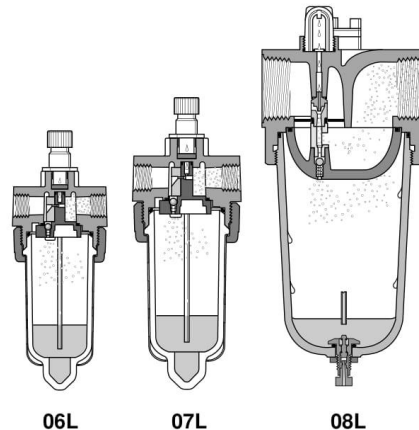
Micro-Mist Air Lubricators are designed to provide optimum and uniform lubrication with fine micro-mist particles of 2 micron or smaller, to pneumatic components even through complex piping arrangements.

- Miniature 14L Series, 1/4 Inch
- Compact 16L Series, 1/4 thru 1/2 Inch
- Standard 17L Series, 3/8 thru 3/4 Inch
- Hi-Flow 18L Series, 3/4 thru 1-1/2 Inch



Lubricator Selection

1. Determine maximum system flow requirements.
2. Determine maximum allowable pressure drop at rated flow in SCFM.
3. Refer to flow chart and select lubricator by choosing the curve that offers minimum pressure drop at desired flow in SCFM.



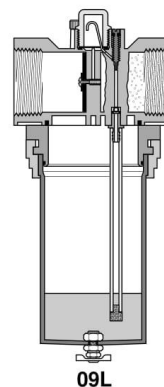
Mist Lubricators

- Pipe Sizes 1/8 thru 2 Inch
- Flows to 1000 SCFM
- Pressures to 250 PSIG



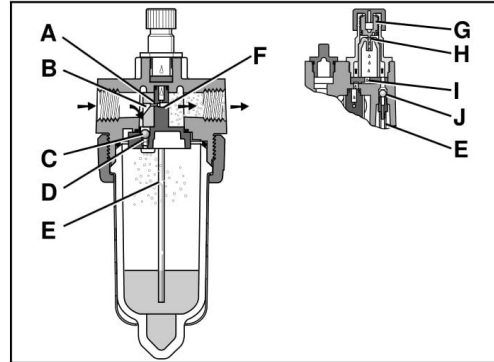
Mist Air Lubricators are designed to provide lubrication for most general applications in a pneumatic system. Units should be installed close to the application ensuring effective distribution of oil to pneumatic components.

- Compact 06L Series, 1/4 thru 1/2 Inch
- Standard 07L Series, 3/8 thru 3/4 Inch
- Hi-Flow 08L Series, 3/4 thru 1-1/2 Inch
- Hi-Flow 09L Series, 2 Inch



Mist Air Line Lubricators Standard 07L Series 3/8, 1/2 & 3/4 Inch—Basic 1/2" Body

Prep-Air II Air Preparation Units



Features

- Proportional oil delivery over a wide range of air flows.
- Precision needle valve assures repeatable oil delivery and provides simple adjustment of delivery rate.
- Bowl can be filled while air line is under pressure.
- Transparent sight dome for 360° visibility.
- Shown with recommended metal bowl guard.

Operation

Air flowing through the unit goes through two paths. At low air flow rates, the majority of the air flows through venturi section (B). The rest of the air slightly deflects and flows by the restrictor disc (A). The velocity of the air flowing through venturi section (B) creates a pressure drop at throat section (F). This lower pressure allows oil to be forced from the reservoir through the pickup tube (E) past the check ball (J), to the metering block assembly where the rate of oil flow is

controlled by metering screw (G). Rotation of the metering screw (G) in the counterclockwise direction increases the flow rate; in the clockwise direction decreases the flow rate. Oil then flows through the clearance between inner and outer sight domes (H) where drops are formed and drip into the throat section (I). Here it is then broken into fine particles and mixed with the swirling air to be carried to the venturi outlet where it joins the air by passing the restrictor disc (A). As air flow rate increases, the restrictor disc (A) deflects, allowing a greater part of the additional air to bypass the venturi section (B). This assures the oil delivery rate increases linearly with increased air flow rate. The check ball (J) assures that when there is no oil flow the oil in the pickup tube does not return to the reservoir.

The bowl can be filled under pressure due to the action of the check ball (C). When the fill cap is removed, air in the bowl escapes and pressure forces the check ball (C) to nearly seal at (D). When the fill cap is replaced, the small amount of air flow past check ball (C) builds up pressure and together with the spring forces the check ball (C) off seat (D), letting full line pressure into the bowl.

Specifications

Body:

Zinc

Bowls:

Transparent Polycarbonate
Metal (Zinc) With Sight Gauge

Bowl Capacity:

6.0 Ounces

Bowl Guard:

Steel

Collar:

Plastic or Metal

Drains:

Manual Twist Drain Standard
Body: Plastic
Nut: Plastic

Injector Meter Block & Base Assy.:

Plastic

Minimum Flow for Lubrication:

.5 SCFM At 100 PSIG

Port Threads:

3/8, 1/2 & 3/4 Inch

Pressure & Temperature Ratings

Polycarbonate Bowl:
0 to 150 PSIG (0 to 10.3 bar)
32°F to 125°F (0°C to 52°C)

Metal Bowl:
0 to 250 PSIG (0 to 17 bar)
32°F to 175°F (0°C to 80°C)

Seals:

Nitrile

Sight Dome:

Polycarbonate

Sight Gauge:

Polyamide

Suggested Lubricant:

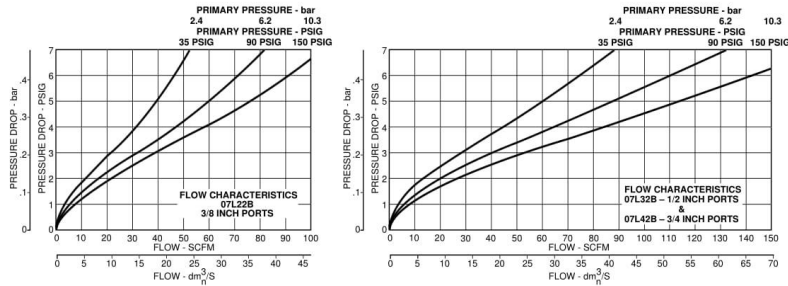
Schrader Bellows F442 Oil

Petroleum based oil of 100 to 200 SSU viscosity at 100°F and an aniline point greater than 200°F.
(DO NOT USE OILS WITH ADDITIVES, COMPOUNDED OILS CONTAINING SOLVENTS, GRAPHITE, DETERGENTS, OR SYNTHETIC OILS.)

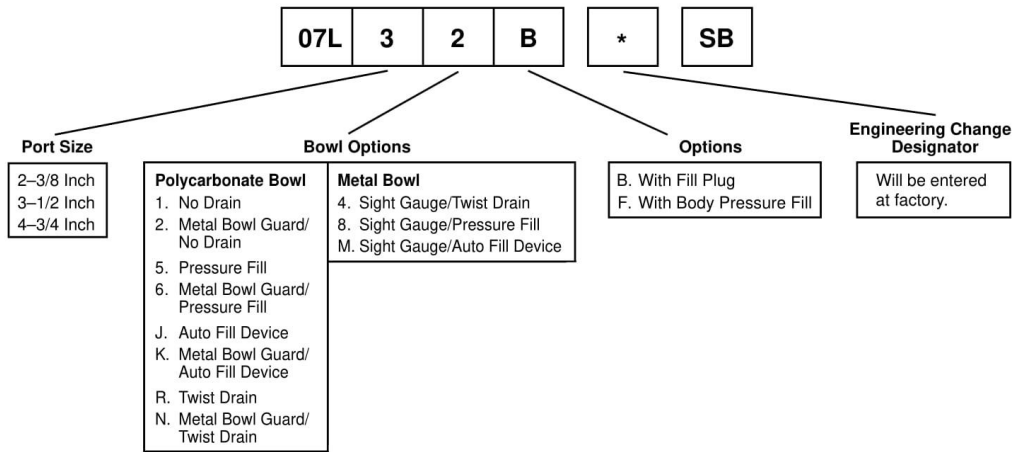
Mist Air Line Lubricators

Prep-Air II Air Preparation Units

Performance Characteristics



Ordering Information



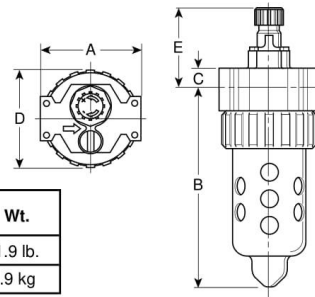
CAUTION:

Polycarbonate bowls, being transparent and tough, are ideal for use with Filters and Lubricators. They are suitable for use in normal industrial environments, but should not be located in areas where they could be subjected to direct sunlight, an impact blow, nor temperatures outside of the rated range. As with most plastics, some chemicals can cause damage. Polycarbonate bowls should not be exposed to chlorinated hydro-carbons, ketones, esters and certain alcohols. They should not be used in air systems where compressors are lubricated with fire-resistant fluids such as phosphate ester and di-ester types.

Metal bowls are recommended where ambient and/or media conditions are not compatible with polycarbonate bowls. Metal bowls resist the action of most such solvents but should not be used where strong acids or bases are present or in salt laden atmospheres. Consult the factory for specific recommendations where these conditions exist.

TO CLEAN POLYCARBONATE BOWLS USE MILD SOAP AND WATER ONLY! **DO NOT** use cleansing agents such as acetone, benzene, carbon tetrachloride, gasoline, toluene, etc., which are damaging to this plastic.

Metal bowl guards are recommended for all applications.



Dimensions:

Model	Port Size Inch	A	B	"B" with Auto-Fill	C	D	E	Wt.
07L	3/8", 1/2", 3/4"	3.24	6.86	7.01	.70	3.25	2.41	1.9 lb.
		82 mm	174 mm	178 mm	18 mm	83 mm	61 mm	.9 kg

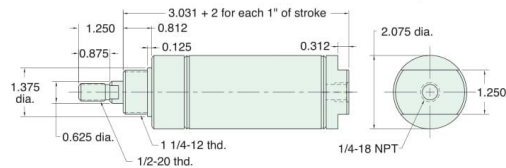
2" BORE STAINLESS STEEL CYLINDER



SSR-32-□-□

Single Acting

Mount: Stud **Standard Stroke Lengths:** 1", 2", 3", 4"
Type: Rotating Rod **Spring Compressed:** 30 lbs. **Spring At Rest:** 15 lbs.
Options: M, B, W, V, N, S **Maximum Stroke:** 20" For M option add 0.125
For S option add 0.375

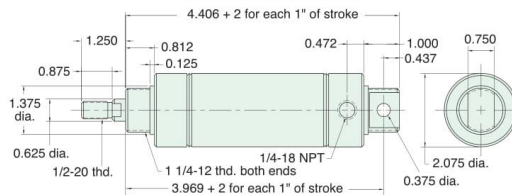


Nut included, but not shown on drawing

USR-32-□-□

Single Acting

Mount: Universal **Standard Stroke Lengths:** 1/2", 1", 1-1/2", 2", 3", 4"
Type: Rotating Rod **Spring Compressed:** 30 lbs. **Spring At Rest:** 15 lbs.
Options: M, B, W, V, N, P6 **Maximum Stroke:** 19" For M option add 0.125

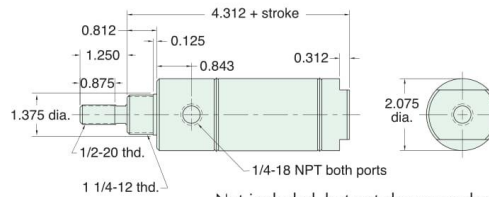


Furnished without nut(s). See Chart on Page 59.

SDR-32-□-□

Double Acting

Mount: Stud **Standard Stroke Lengths:** 1/2", 1", 1-1/2", 2", 3", 4", 5", 6"
Type: Rotating Rod **Maximum Stroke:** 39"
Options: C, F, R, M, B, W, V, N, S, P6, P7, P8 For C, F, R and S options add 0.375



Nut included, but not shown on drawing
 C, F, & R options use side ported rear head

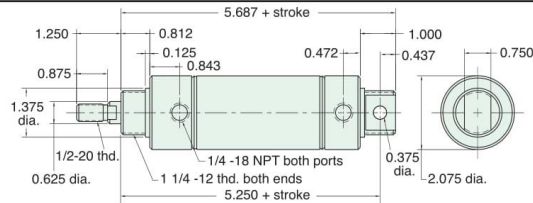
UDR-32-□-□

Double Acting

Mount: Universal **Standard Stroke Lengths:** 1/2", 1", 1-1/2", 2", 3", 4", 5", 6", 7", 8", 10", 12"
Type: Rotating Rod **Maximum Stroke:** 38"
Options: C, F, R, M, B, W, V, N, P2, P3, P4, P5, P6, P7, P8



New All Stainless Steel line
 now available!
 See [pages 66 - 70](#)



Furnished without nut(s). See Chart on Page 59.

Pneumatic Division
 Richland, Michigan 49083
 269-629-5000

Installation & Service Instructions
V235

Quick Exhaust and Shuttle Valve

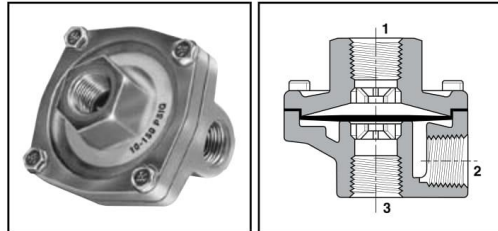
ISSUED: June, 2009
Supersedes: None

Doc.# V235, EN# 090471, Rev. 1

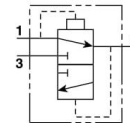
⚠ WARNING

To avoid unpredictable system behavior that can cause personal injury and property damage:

- Disconnect electrical supply (when necessary) before installation, servicing, or conversion.
- Disconnect air supply and depressurize all air lines connected to this product before installation, servicing, or conversion.
- Operate within the manufacturer's specified pressure, temperature, and other conditions listed in these instructions.
- Medium must be moisture-free if ambient temperature is below freezing.
- Service according to procedures listed in these instructions.
- Installation, service, and conversion of these products must be performed by knowledgeable personnel who understand how pneumatic products are to be applied.
- After installation, servicing, or conversion, air and electrical supplies (when necessary) should be connected and the product tested for proper function and leakage. If audible leakage is present, or the product does not operate properly, do not put into use.
- Warnings and specifications on the product should not be covered by paint, etc. If masking is not possible, contact your local representative for replacement labels.



Symbol



General Information

Quick exhaust valves provide rapid exhaust of control air when placed between control valve and actuator. They can also be used as shuttle valves. Diaphragm materials are available in urethane, Nitrile, Fluorocarbon, and PTFE to meet a wide variety of operating conditions.

Valve Specifications

Operating Pressure (Air)
 Maximum: 150 PSIG
 200 PSIG for Model No. 0R37TB
 (PTFE diaphragm)
 Minimum: 3 PSIG
 50 PSIG for Model No. 0R37TB
 (PTFE diaphragm)

Operating Temperature

Urethane: 0°F to 180°F* (-18°C to 80°C)
 Nitrile: 0°F to 180°F* (-18°C to 80°C)
 Fluorocarbon: 0°F to 400°F* (-18°C to 205°C)
 PTFE: 0°F to 500°F* (-18°C to 260°C)
 * Ambient temperatures below freezing require moisture-free air. Ambient temperatures below freezing and above 180° require lubricants especially selected for suitability at these temperatures. Pneumatic valves should be used with filtered and lubricated air.

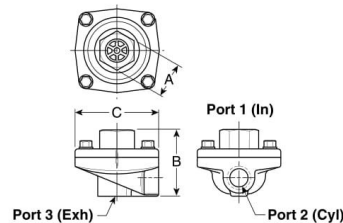
Component Materials

Body Material: Die cast aluminum
Static Seals: Nitrile standard with urethane
 (Others see below)
 Nitrile - 7/8" Sq.
Diaphragm: Standard – Urethane - 1" & 1-1/2" Hex
 Optional – Fluorocarbon, PTFE,
 or Nitrile (Depending on size)

Mounting Bracket Kit –

No. 03640 8100
 (Including body screws)

For "0R12" and "0R25" sizes.



⚠ WARNING

FAILURE OR IMPROPER SELECTION OR IMPROPER USE OF THE PRODUCTS AND/OR SYSTEMS DESCRIBED HEREIN OR RELATED ITEMS CAN CAUSE DEATH, PERSONAL INJURY AND PROPERTY DAMAGE.

This document and other information from The Company, its subsidiaries and authorized distributors provide product and/or system options for further investigation by users having technical expertise. It is important that you analyze all aspects of your application, including consequences of any failure and review the information concerning the product or systems in the current product catalog. Due to the variety of operating conditions and applications for these products or systems, the user, through its own analysis and testing, is solely responsible for making the final selection of the products and systems and assuring that all performance, safety and warning requirements of the application are met.

The products described herein, including without limitation, product features, specifications, designs, availability and pricing, are subject to change by The Company and its subsidiaries at any time without notice.

EXTRA COPIES OF THESE INSTRUCTIONS ARE AVAILABLE FOR INCLUSION IN EQUIPMENT / MAINTENANCE MANUALS THAT UTILIZE THESE PRODUCTS. CONTACT YOUR LOCAL REPRESENTATIVE.

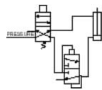
Model Selection, Performance Data and Dimensions

Port			Flow (SCFM†)	Model Number		A	B	C	Service Kit No.
1	2	3		NPTF	BSPF "G"				
STANDARD URETHANE DIAPHRAGMS (Nitrile static seals)									
1/4"	1/4"	3/8"	150	OR25NB	ORB25NB	1" Hex	2.06	2.44	03340 0105
	3/8"	3/8"	240	OR25PB	—	1" Hex	2.06	2.44	03340 0105
3/8"	3/8"	3/8"	240	OR37B	ORB37B	1" Hex	2.06	2.44	03340 0105
1/2"	1/2"	1/2"	450	OR50B	ORB50B	1-1/2" Hex	2.88	3.38	03475 0109
3/4"	3/4"	3/4"	550	OR75B	ORB75B	1-1/2" Hex	2.88	3.38	03475 0109
NITRILE DIAPHRAGMS (Nitrile static seals)									
1/8"	1/8"	1/8"	70	OR12B	ORB12B	7/8" Sq.	1.75	1.88	03640 8000
	1/8"	1/4"	70	OR12NB	ORB12NB	7/8" Sq.	1.75	1.88	03640 8000
1/4"	1/4"	1/4"	90	OR25B	ORB25B	7/8" Sq.	1.75	1.88	03640 8000
	1/4"	3/8"	90	OR25NFB	ORB25NFB	7/8" Sq.	1.75	1.88	03340 8000
3/8"	3/8"	3/8"	240	OR37FB	ORB37FB	1" Hex	2.06	2.44	03340 8000
3/4"	3/4"	3/4"	550	OR75FB	ORB75FB	1-1/2" Hex	2.88	3.38	03475 9000
FLUOROCARBON DIAPHRAGMS for extended temperature operation (Fluorocarbon static seals)									
1/8"	1/8"	1/8"	70	OR12VB	ORB12VB	7/8" Sq.	1.75	1.88	03650 8000
	1/8"	1/4"	70	OR12NVB	ORB12NVB	7/8" Sq.	1.75	1.88	03650 8000
1/4"	1/4"	1/4"	90	OR25VB	ORB25VB	7/8" Sq.	1.75	1.88	03650 8000
3/8"	3/8"	3/8"	240	OR37VB	ORB37VB	1" Hex	2.06	2.44	03340 0319
1/2"	1/2"	1/2"	450	OR50VB	ORB50VB	1-1/2" Hex	2.88	3.38	03475 0120
3/4"	3/4"	3/4"	550	OR75VB	ORB75VB	1-1/2" Hex	2.88	3.38	03475 0120
PTFE DIAPHRAGMS for higher pressure and temperature (Fibre static seals)									
3/8"	3/8"	3/8"	240	OR37TB	ORB37TB	1" Hex	2.06	2.44	03340 0504

† At 100 PSIG inlet pressure with full pressure drop.

BOLD ITEMS ARE MOST POPULAR.

Typical "Quick Exhaust Valve" Applications



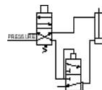
Rapid Retraction – Double Acting Cylinder

In this circuit, air is exhausted through a Quick Exhaust Valve that is **close coupled** to the cap end of the cylinder. Because the Quick Exhaust Valve has a greater exhaust capacity than the four-way Control Valve, increased cylinder speed can be accomplished with a smaller and less expensive control valve.

Dual Pressure Actuation of Double Acting Cylinder

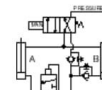
This circuit utilizes a Quick Exhaust Valve and a three-way Control Valve to permit rapid extension of the cylinder at a high pressure. Retraction can be accomplished at a lower pressure, thus saving air and increasing cylinder life.

NOTE: Line pressure must be 3 or 4 times greater than rod end pressure. Effective working pressure is the differential between the cap and rod end.

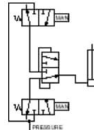


Bi-Directional Control of Two Double Acting Cylinders

This circuit provides maximum control with a minimum of valving. A large four-way Control Valve is not needed to permit the rapid retraction of Cylinder A, as the Quick Exhaust Valve performs this function. The extension of Cylinders A and B and retraction of Cylinder B are controlled by Speed Control Valves.

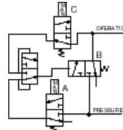


Typical "Shuttle Valve" Applications



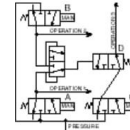
"OR" Circuit

The most common application of the Shuttle Valve is the "OR" Circuit. Here a cylinder or other work device can be actuated by either control valve. The valves can be manually or electrically actuated and located in any position.



Memory Circuit

This circuit enables continuous operation once initiated. Pressure is delivered to the circuit when Valve A is actuated. This allows pressure to pass through the shuttle valve actuating Valve B. Pressure then flows through Valve B and also the other side of the shuttle valve which holds Valve B open for continuous operation. To unlock the circuit, Valve C must be opened to exhaust the circuit and allow Valve B to return to its normally closed position.



Interlock

This circuit prevents the occurrence of a specific operation while one or another operation takes place. When either Valve A or B is actuated to perform operation 1 or 2, Valve D is shifted to the closed position and prevents operation 3 from occurring.

Catalog PDN1000-2US
Parker Pneumatic

Air Preparation Products
06R, 07R General Industrial Regulators

- Secondary aspiration plus balanced poppet provides quick response and accurate pressure regulation
- Rolling diaphragm for extended life
- Two high flow 1/4" gauge ports can be used as additional outlets
- Easily serviced
- Removable non-rising knob for panel mounting and tamper resistance
- 06R: 1/4", 3/8" & 1/2" ports (NPT & BSPP)
- 07R: 1/2" & 3/4" ports (NPT & BSPP)



Material specifications

Adjusting Stem	Steel
Body	Zinc
Bonnet, piston stem, valve poppet & cap	Plastic
Collar, knob	Plastic
Diaphragm	Nitrile
Seals	Nitrile
Springs – Poppet	Stainless
Control	Steel

Operating information

	06R (Compact), 07R (Standard)
Pressure rating:	250 PSIG (17.2 bar)
Temperature rating:	32°F to 175°F (0°C to 80°C)
Secondary pressure ranges –	
Standard pressure	2 to 125 PSIG (0 to 8.6 bar)
Medium pressure	1 to 60 PSIG (0 to 4.1 bar)
High pressure	5 to 250 PSIG (0.4 to 17.2 bar)
For technical information see CD	

Regulators



	Port size	Pressure range	Flow SCFM	Part number (NPT)	
				Without gauge	With 160 PSI gauge
06R 	1/4"	125 PSIG	53	06R113AC	06R118AC
	3/8"	125 PSIG	60	06R213AC	06R218AC
	1/2"	125 PSIG	75	06R313AC	06R318AC
07R 	1/2"	125 PSIG	90	07R313AC	07R318AC
	3/4"	125 PSIG	90	07R413AC	07R418AC

WARNING
 Product rupture can cause serious injury.
 Do not connect regulator to bottled gas.
 Do not exceed maximum primary pressure rating.

CAUTION:
REGULATOR PRESSURE ADJUSTMENT –
 The working range of knob adjustment is designed to permit outlet pressures within their full range. Pressure adjustment beyond this range is also possible because the knob is not a limiting device. This is a common characteristic of most industrial regulators, and limiting devices may be obtained only by special design. For best performance, regulated pressure should always be set by increasing the pressure up to the desired setting.

Most popular.



E65

Parker Hannifin Corporation
 Pneumatic Division
 Richland, Michigan
www.parker.com/pneumatics

E

General Industrial
 Air Preparation Products

Liquid
 Separators

Particulate
 Filters

Coalescing
 Filters

Regulators

Pilot
 Regulators

Filter /
 Regulators

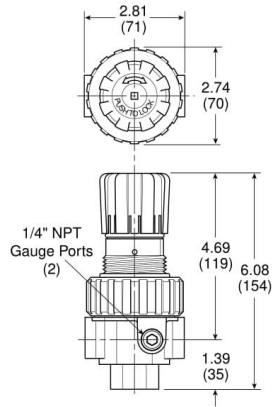
Micro-Mist
 Lubricators

Mist
 Lubricators

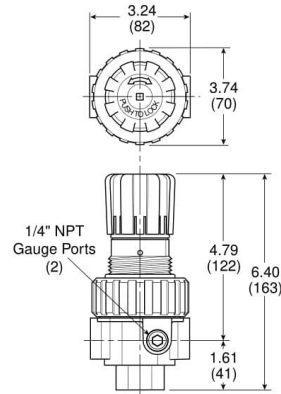
Combinations

- E
- General Industrial
Air Preparation Products
- Liquid
Separators
- Particulate
Filters
- Coalescing
Filters
- Regulators
- Pilot
Regulators
- Filter/
Regulators
- Micro-Mist
Lubricators
- Mist
Lubricators
- Combinations

06R (Compact)



07R (Standard)



Service kits

Description	06R (Compact)	07R (Standard)
Bonnet assembly	PS715P	PS715P
Control knob	P04069B	P04069B
Gauges –		
60 PSIG (0 to 4.1 bar)	K4520N14060	K4520N14060
160 PSIG (0 to 11.0 bar)	K4520N14160	K4520N14160
300 PSIG (0 to 20.0 bar)	K4520N14300	K4520N14300
Mounting bracket kit (Includes panel mount nut)	PS707P	PS807P
Panel mount nut –		
Plastic	P04082	P04079B
Metal	P04082	P04079B
Reverse Flow Service Conversion Kit – Relieving	PS708RP	PS808RP
Springs –		
1-30 PSIG range	P01698	P01698
1-60 PSIG range	P04062	P04062
2-125 PSIG range	P04063	P04063
5-250 PSIG range	P04064	P04064
Tamperproof kit	PS737P	PS737P

Most popular.



E66

Parker Hannifin Corporation
 Pneumatic Division
 Richland, Michigan
www.parker.com/pneumatics

APPENDIX B

APPENDIX B

WAYSIDE HBD ARDUINO CODE

```
#define FOURWAYVALVE 8
#define SENSORPINONE 12
#define SENSORPINTWO 7

unsigned long time1, time2;
int count=0; //LEAVE THIS VALUE ALONE

void setup() {
  pinMode(FOURWAYVALVE, OUTPUT);
  pinMode(SENSORPINONE, INPUT);
  pinMode(SENSORPINTWO, INPUT);
  digitalWrite(SENSORPINONE, HIGH);
  digitalWrite(SENSORPINTWO, HIGH);
  Serial.begin(9600);
}

void loop(){

  if (digitalRead(SENSORPINONE) == LOW) {
    time1=millis();
    Serial.println("stepone");

    while (true){
      if (digitalRead(SENSORPINTWO) == LOW){
        digitalWrite(FOURWAYVALVE,LOW);
        time2=millis();
        break;
      }
      else {
        Serial.println("steptwo");
        //count = count+1;
      }
    }
  }
}
```

```
    Serial.print(time2);
    Serial.print(', ');
    Serial.println(time1);
    delay(30000);
}
else {
    digitalWrite(FOURWAYVALVE, HIGH);
    Serial.println("step0");
}
}
```

REFERENCES

- [1] Anderson, G. B. "Acoustic detection of distressed freight car roller bearing", *Proceedings of the 2007 JRCICE Spring Technical Conference*, Pueblo, Colorado, March 13–16, (2007).
- [2] Wiley, R. B. and Snyder, T. Technical Report, "From ATSI to TDTI: Existing Technologies Analysis and Statistical Review Future Technologies", Transportation Technology Center, Inc. and Union Pacific Railroad, (2011).
- [3] "Predicting Hot Box Detector Failures," *Predikto*. [Online]. Available: https://www.predikto.com/download/Predikto_CaseStudy_Railroad_HBD.pdf [Accessed 10 Oct 2018].
- [4] Tabbachi, J.G., Newman, R.R., Leedham, R.C., Purta, D.A., Madered, G.G., Galli, R. "Hot Bearing Detection with the SMART-BOLT." *Proceedings of the 1990 ASME/IEEE Joint Railroad Conference*, p. 105-10. 1990. Print.
- [5] Karunakaran, S., Snyder, T.W., 2007, "Bearing temperature performance in freight cars," *Proceedings Bearing Research Symposium*, sponsored by the AAR Research Program in conjunction with the ASME RTD Fall Conference, Chicago, IL, September 11-12.
- [6] Ose, Mixanikos. "Heat Detectors-box and Brake Disc (Hot Box & Hot Wheel Detection System)." N.p., 16 July 2015. Web. 17 Jan. 2017.
- [7] "Tapered Roller Bearing Units TAROL Products and Services." Schaeffler. www.schaeffler.com/remotemedien/media/_shared...2/.../tpi_158_de_en.pdf, Date Last Accessed: 12 Dec. 2016
- [8] Cline, J., Bonetto, A, 2015, "Evaluation of Hot Bearing Detector Technology Used to Identify Bearing Temperatures," AAR Research Report, R-1009.
- [9] "Federal Railroad Administration Office of Safety Analysis." [Online]. Available:<https://safetydata.fra.dot.gov/OfficeofSafety/default.aspx> [Accessed 10 Feb 2017].
- [10] A. Schobel, M. Pisek and J. Karner, "Hot Box Detection Systems as a Part of Automated Train Observation in Austria," *Towards the competitive rail systems in Europe*, pp. 157-161, 31 May 2006.
- [11] Lagneböck, Robert. *Evaluation of wayside condition monitoring technologies for condition-based maintenance of railway vehicles*. Diss. Luleå tekniska universitet,

2007.

- [12] Lunys, Olegas, Stasys Dailydka, and Gintautas Bureika. "Investigation on features and tendencies of axle-box heating." *Transport problems* (2015).
- [13] D. Barke and W. K. Chiu, "Structural health monitoring in the railway industry: A review," *Struct. Health Monitor.*, vol. 4, no. 1, pp. 81–93, 2005.
- [14] Judge, T. "Searching for a hot one." *Railway Age* 205.1 (2004).
- [15] Cline, J., Bonetto, A., and Sultana, T., 2014, "Evaluation of Hot Bearing Detector Technology Used to Identify Bearing Temperatures," *Technology Digest*, TD-14-017.
- [16] Transportation Safety Board of Canada, 1999, "Derailment," *Railway Investigation Report*, R99T0031.
- [17] Cackovic, David L., et al. "Hot Bearing Detector Specification Test: Report No. R-750." *Rail Transportation: Presented at the Winter Annual Meeting of the American Society of Mechanical Engineers*. ASME, 1991.
- [18] Ouyang, Y., Belpert, S., and Clasby, D., 2017, "Spacing Study of Hot Bearing Detectors," *Technology Digest*, TD-17-034.
- [19] Tarawneh, C., Mealer, A., and Crown, S., 2017, "Radiative Heat Transfer Analysis of Railroad Bearings for Wayside Hot-Box Detector Optimization", *Proceedings of the 2017 Joint Rail Conference*, Philadelphia, PA, April 4-7.
- [20] Tarawneh, C., Aranda, J., Hernandez, V., and Ramirez, C., "An Analysis of the Efficacy of Wayside Hot-Box Detector Data," *Proceedings of the 2018 ASME Joint Rail Conference*, Pittsburgh, PA, April 18-20, 2018.
- [21] Tarawneh, C., Kypuros, J.A., Wilson, B.M., Snyder, T.W., Gonzalez, B., and Fuentes, A.A., 2009, "A Collaborative On-Track Field Test Conducted to Verify the Laboratory Findings on Bearing Temperature Trending," *Proceedings of the 2009 ASME Joint Rail Conference*, JRC2009-63056, Pueblo, CO, March 3-5.
- [22] Tarawneh, C., Sotelo, L., Villarreal, A., De Los Santos, N., Lechtenberg, R., and Jones, R., 2016, "Temperature Profiles of Railroad Tapered Roller Bearings with Defective Inner and Outer Rings," *Proceedings of the 2016 Joint Rail Conference*, Columbia, SC, April 12-15.

BIOGRAPHICAL SKETCH

James Aranda was born in Mission, Texas on September 27, 1995. He attended Sharyland High school and graduated in the Spring of 2013. Afterwards, he attended the University of Texas Rio Grande Valley, where he graduated Summa Cum Lade with a bachelor's degree in Mechanical Engineering in the Fall of 2016. During his last semester, James was also selected as the Outstanding Undergraduate Student for the Mechanical Engineering department. He later chose to continue his studies at the University of Texas Rio Grande Valley and obtained his Master of Science degree in Mechanical Engineering in December 2018. During this time, James co-authored two research papers and was named the 2017 Student of the Year for the University Transportation Center for Railway Safety. James may be reached by email at alexaranda46@gmail.com.